REPORT R-403 JANUARY, 1969

CSL COORDINATED SCIENCE LABORATORY

ELECTRICAL PROPERTIES OF SOME VACUUM DEPOSITED INSULATING FILMS

OWEN REILLY

UNIVERSITY OF ILLINOIS – URBANA, ILLINOIS

This work was supported in part by the Joint Services Electronics Program (U.S. Army, U.S. Navy, and U.S. Air Force) under Contract DAAB 07-67-C-0199; and in part by Army DAAK-02-67-C-0546.

Reproduction in whole or in part is permitted for any purpose of the United States Government.

Distribution of this report is unlimited.

ACKNOWLEDGMENTS

I wish to express my sincere appreciation to Professor R. N. Peacock for suggesting this timely area of research and for his patient and able guidance. His policy of minimal intervention in thesis research has encouraged me through this survey to develop areas of strong curiosity for the furtherance of my learning. I could ask nothing higher of the profession of teaching.

It is my hope that this work has furthered the long tradition of communication between physics and electrical engineering. Should such be the case, Professor Peacock has effected it.

Wishing to be brief, I thank only my wife, Clara, for entering much data into the log, Mr. Steven Depp, for helping with the draft revisions, Dr. J. T. Jacobs, for giving me an introduction to vacuum technology, the Coordinated Science Laboratory, which provided the technical services and supported the work, and other members of the Applied Physics Group, who assisted through many consultations.

TABLE OF CONTENTS

CHAPTER | Page

INTRODUCTION 1

I CONDUCTION THEORY 2

The M-I-M Structure--Representation of Trapping in Insulators 2
The Effects of Trapping in Insulators 3
The Biased M-I-M Structure--Space-Charge-Limited Currents 4
The Biased M-I-M Structure--Tunneling Currents 8
The Biased M-I-M Structure--Schottky Emission Currents 9
The Biased M-I-M Structure--Breakdown 10
Low Bias Thick Film and Bulk Resistivity Description 10
The Stability of Insulators 11
Forming Curves 11

II DESCRIPTION OF EXPERIMENTS AND EQUIPMENT 13

Geometry of Samples 14
The Choice of Electrodes 14
Description of the Vacuum System 15
Deposition Methods Used 17
Thickness Monitors 19
Decomposition 22
Evaporation of $ThOF_2$ 22
Types of Measurements 22
Self-Healing Breakdown Technique of Measuring Maximum Voltages and Pinholes 24
Comparison of Electron Beam and Filament Evaporation 25
Conclusions and Data 25

APPENDIX HIGH TEMPERATURE OXIDES AND NITRIDE 53

REFERENCES 54

LIST OF TABLES

Table Page

1. Summary of Parameters 27

2. Filament Evaporated Insulators ~300 Å thick. 28

3. Electron Beam Deposited Insulators ~300 Å thick. 29

4. Filament Evaporated Insulators ~5000 Å thick. 30

5. Electron Beam Deposited Insulators ~5000 Å thick. 31

LIST OF FIGURES

Figure | Page

1. Energy band diagram of an M-I-M structure at zero bias, showing the heights of the insulator forbidden gap above the Fermi levels. 32

2. Energy band diagram of an insulator showing the increase in occupation of a continuum of trapping levels due to injected electrons. 33

3. Experimental long-term discharge current from a Al-SiO_2-Si structure. The SiO_2 (6000 Å) was thermally grown. (From Lindmayer & Wrigley, Fundamentals of Semiconductor Devices, D. Van Nostrand Co., Princeton, N.J., 1964, p. 442.) 34

4. Best fit curve through computer generated points for the electron distribution in an insulator for one-carrier space-charge limited current. The ordinate applies to the normalized current of magnitude 10. For the normalized current of 100 the vertical scale should be multiplied by five, and by 100 for the normalized current of 10,000. (From Lindmayer & Wrigley, Fundamentals of Semiconductor Devices, p. 436.) . . . 35

5. Energy diagram band of an insulator showing the increase in occupation of a single trapping level due to injected electrons. 36

6. Energy band diagram for a biased M-I-M structure showing a single carrier (electron) space charge. An approximate relation for the current is $J = 9\varepsilon\varepsilon_o qV_a^2/8d^3$. 37

7. Best fit curve through computer generated points for the current-voltage relation for one-carrier space-charge limited current. For practical voltages the characteristic is quadratic. (From Lindmayer & Wrigley, Fundamentals of Semiconductor Devices, p. 435.) 38

8. Current-voltage relation showing hysteresis in an Al-SiO_2-Si structure. The SiO_2 (5000 Å) was thermally grown. (From S. M. Hu, J. Electrochemical Soc. 113, 697 (1966). 39

9. Slow sweep rate current-voltage relation for an Al-TiO-Al structure. The TiO (~100 Å) was electron beam deposited. Some decomposition probably occurred causing the extraordinarily low resistance. The current follows closely $J \propto V_a^2$ showing the space-charge-limited effect. 40

10. Energy band diagram for a biased M-I-M structure where the insulator is thin enough for the electrons to penetrate by direct quantum mechanical tunneling. 41

Figure Page

11. Energy band diagram for a biased M-I-M structure where the bias is great enough for the effective barrier thickness to be reduced. This leads to Fowler-Nordheim tunneling. 42

12. Low voltage theoretical tunnel resistance vs. thickness for various barriers corrected for image forces. SiO_x tunnel resistance has been plotted from estimates based on a barrier height $\phi = 3$ and dielectric constant of 4. The range of experimental resistances for Al-SiO_x-Al structures is expected to lie to the right and below the SiO_x lines shown above. (From J. G. Simmons, J. Appl. Phys., 34, 1802 (1963).) 43

13. Low voltage resistance vs. thickness for 40 samples from five slides. For comparison the bulk resistance and tunnel resistance curves from Fig. 12 have been reproduced. Thickness was measured using a crystal monitor and "geometric leverage." 44

14. Slow sweep rate current-voltage relation for an Al-$ThOF_2$-Al structure. The $ThOF_2$ (900 Å) was electron beam deposited. The negative resistance which appears here is a result of the forming and is non-repeatable. These results, taken on an X-Y plotter, are typical of the type obtained when applied fields are high enough to cause forming but not high enough to cause destructive breakdown. All four sweeps were started at the points marked (0,0) and are separated for clarity. For less than 5 volts applied, the current is in the nanoampere range. 45

15. Slow sweep rate current-voltage relation for Al-$ThOF_2$-Al structure. The $ThOF_2$ (900 Å) was electron beam deposited. The negative resistance which appears here is a result of the forming and is non-repeatable. At lower currents than those resolvable on this curve the D.C. current-voltage relation after forming is repeatable. All three sweeps were started at the points marked (0,0). 46

16. Al-Ins.-Al structure forming curves (first application of voltage) for vacuum deposited insulators. Breakdowns, when observed, are shown with arrowheads. The base electrode was deposited ≃1500 Å thick and the counterelectrode deposited ≃800 Å thick. See tables for information about each insulator. 47

17. Al-Ins.-Al structure forming curves (first application of voltage) for vacuum deposited insulators. Breakdowns, when observed, are shown with arrowheads. The base electrode was deposited ≃1500 Å thick and the counterelectrode deposited ≃800 Å thick. See tables for information about each insulator. 48

Figure Page

18. Slow sweep rate current-voltage relations for three Al-CeO-Al structures on the same slide. The cerium oxide (~100 Å) was electron beam deposited. M-I-M structures simultaneously deposited on the same slide showed dc resistance variations of at least this magnitude for all insulators tested. 49

19. Schematic representation of the vacuum system to be shown in Fig. 20. 50

20. A commercial diffusion pumped vacuum system with bell jar raised, showing an electron beam deposition unit power supply. 51

21. Photograph of the hardware used for deposition. From left to right: high voltage feedthrough, micrometer leak valve, MRC electron beam gun, watercooling feedthrough, Drumheller source, and five tungsten or molybdenum boats. 52

INTRODUCTION

Materials can be classified as conductors, semiconductors, or insulators. The distinguishing difference among these classes is the resistivity. Conductors generally have resistivities of the order of 10^{-5} ohm-cm; semiconductors fall in a range around 1 ohm-cm; and insulators have resistivities near 10^{10} ohm-cm. This large difference in resistivity of the three classes of materials is the basis of their engineering applications. The resistivities of all three classes may be functions of many parameters, including temperature, purity, conditions of preparation, and the field strengths applied to them. The experimentally determined resistivities for a group of vacuum deposited thin film insulators will be presented in this paper.

This work will briefly discuss the theory of conductivity for insulators and present experimental data showing current-voltage characteristics for several thin film, vacuum deposited, insulators. The maximum electric fields which could be applied to the films will also be given along with the yield of "unshorted" structures and the maximum thickness obtained on room temperature substrates. Finally, the method of sample preparation will be described, including the electrodes and substrate chosen and equipment used for deposition. These parameters are of growing interest for users of insulators. Both the development of new devices and improvement of existing ones are assisted by increased knowledge of thin film isolation technology.

CHAPTER I

CONDUCTION THEORY

Figure 1 shows the energy band diagram for the arbitrary metal-insulator-metal (M-I-M) structure. Here, the barrier represents an ideal trap-free insulator. When dissimilar metals are used for the electrodes, the barrier height will be different on the right and left sides. This is because the work functions of the two metals are in general different. The dissimilar electrode model predicts asymmetrical I-V characteristics.[1] Since aluminum electrodes are commonly used for data reported in the literature, and because of technological advantages to be described later, only similar electrodes will be discussed in the theory, and only similar aluminum electrode data will be presented.

Assuming like electrodes and a simple rectangular barrier in the insulator, and neglecting image forces for the present, $\phi_1 = \phi_2 = \phi$. Thus the model becomes symmetrical,[1,2] a justified simplification as verified by experiment in this work.

The M-I-M Structure--Representation of Trapping in Insulators

Films formed by vacuum deposition are generally polycrystalline or amorphous, and their band model can be represented by the usual picture with the addition of a continuum of trapping levels throughout the forbidden gap (Fig. 2).[3] These trapping levels capture injected electrons for varying lengths of time, depending on their depth, and trapping can greatly reduce the current through the insulator.[4,5] As will be shown, the filled traps strongly affect the Fermi level because there are few free electrons remaining for conduction.

The Effects of Trapping in Insulators[3,6]

The insulators used in this work were all vacuum deposited with either a filament or electron beam source. As was stated above, such films contain a significant number of "traps." These traps are allowed energy levels in the forbidden energy gap. The occupation of the trapping levels can be found from the results obtained for impurities. Thus we can write

$$n_t = N_T/\{\tfrac{1}{2} \exp [-(E_f - E_T)/KT] + 1\}$$

where N_t is the trapping site density.[3,7,8,9] Thus, for a trapping level several KT units above the Fermi level,

$$n_t \simeq 2N_T \exp (E_f - E_T)/KT$$

Also from semiconductor theory, we know that the concentration of electrons in the conduction band can be written as

$$n = N_c \exp [(E_f - E_c)/KT]$$

where N_c is the state density in the conduction band $\simeq 10^{19}/cm^3$. Combining the expressions for n and n_t, we find

$$n/n_t = \frac{N_c}{2N_T} \exp [(E_T - E_c)/KT]$$

which will generally be very small since the depth of trapping levels for insulators can be quite deep. This equation, with the mobility equation, $\mu^* \simeq \frac{n}{n_t} \mu$, which will be described in a later section, also implies that the mobility is greatly reduced when deep traps are present and that their discharge will take a long time. This is seen in Fig. 3 for a Si-SiO_2-Al structure.[3] This current, representing only a fraction

of the trapped electrons, demonstrates the presence of traps with discharge times of 20 minutes or more.

The reason that only a fraction of the trapped electrons are observed can be explained with the aid of Figs. 3 and 4.[3] More traps are filled at the negative electrode (assuming electron traps only) than at the positive electrode. When the external circuit is shorted, electrons slowly move toward both electrodes as the traps empty; however, more electrons will go to the negative electrode than to the positive electrode because traps were filled to higher levels there. The net difference in the rate at which electrons reach the two electrodes can be recorded by using an ammeter as the shorting device.

Those traps nearest the plates empty first, enabling one to envision creating a ripple-type quasi Fermi level across the insulator, due to alternately applying and removing the voltage.

The Biased M-I-M Structure--Space-Charge-Limited Currents[3,6,10]

Figure 5 is the energy level diagram of an insulating film. Fig. 6 represents a biased trap-free M-I-M structure to be used as a model for the calculations which follow. Following Lindmayer and Wrigley,[3] it is assumed that the current is primarily a drift current of electrons (single carrier case); hence

$$J = q\mu E n$$

Since the electrons are the only carriers, the space-charge density in the insulator is qn, and Poisson's equation then becomes

$$dE/dx = -qn(x)/\varepsilon\varepsilon_o$$

From these equations

$$-J = \mu\varepsilon\varepsilon_o E dE/dx = \frac{1}{2}\mu\varepsilon\varepsilon_o (dE^2/dx)$$

This can be integrated by noting that only E is dependent upon x, so that

$$E(x) = \sqrt{2(-Jx + c)/\mu\varepsilon\varepsilon_o}$$

The integration constant, c, can be set equal to zero, since for truly space-charge-limited conditions the field at x = 0 is nearly zero. This evaluation is valid because the term "space-charge-limited" means that the injected electrons themselves reduce the electric field near the injecting contact. We now obtain

$$E(x) = \sqrt{2Jx/\mu\varepsilon\varepsilon_o}$$

by noting that since the actual current is negative, the negative sign on J has no significance. This can be integrated to give the voltage across the sample.

$$V_a = \int_0^d E(x)dx$$

from which

$$J = 9\mu\varepsilon\varepsilon_o V_a^2/8d^3$$

Note that since the mobility, μ, is not very temperature dependent in the insulator, this space-charge-limited current is far less temperature dependent than injection currents in semiconductor p-n junctions. The injected current is only weakly dependent upon changes in the Fermi levels.

The assumption made early in this section that J may be taken as drift current is shown by Fig. 7 to be valid for voltages above 0.25 volts.

The space-charge-limited currents modify the Fermi level in the insulator for two reasons. The first is the electron spatial distribution. The second is the result of the filling of electron traps. As the injected electron concentration increases, at some distance into the insulator, x, the trapping levels in the insulator fill. As the voltage is decreased, the filled traps empty with a finite discharge time. The time dependent trap charging and discharging cause two effects on the I-V characteristics. The first is to reduce space-charge-limited currents and the second is either to produce ac hysteresis (see Fig. 8), or when observed under dc conditions, time dependent current decay at zero voltage (see Fig. 3).

The reduction in space-charge-limited current caused by traps can be handled approximately by breaking up the electron concentration into free and trapped components, n and n_t, respectively. It is then possible to define an effective mobility, μ^*, by the relation

$$n\mu = (n + n_t)\mu^*$$

and repeat the derivation for space-charge-limited current using both the free and trapped electron concentrations. These steps result in a current

$$J = 9\mu^* \varepsilon\varepsilon_o V_a^2/8d^3$$

so the trap free current has been effectively reduced by the ratio

$$\frac{\mu^*}{\mu} = \frac{n}{n+n_t}$$

Since n_t is found to be much greater than n for most amorphous and polycrystalline insulators,

$$\frac{\mu^*}{\mu} \simeq \frac{n}{n_t}$$

As an example, for one of the samples in this experiment the equation for trap-free conduction predicted 10^5 times more current than was actually observed.

Mobility is also related to the trapping. The time an electron loses in a trap serves to reduce the net motion of the electron. Because trapping is dominant in vacuum deposited insulators, mobilities may be as low as 0.01 cm^2/volt-sec. The trapping ratio, n/n_t, cannot be given for a film without qualification as to the deposition conditions and substrate used, since these parameters strongly affect the value obtained. Thus, trapping sites greatly reduce space-charge-limited currents. For this reason it is difficult to correlate space-charge-limited currents with theory unless the mobility reduction factor can be determined. Figure 9 shows an experimental current-voltage characteristic for an Al-TiO-Al structure where the current is believed to be space-charge-limited.

The time dependent current decay in Fig. 3 due to traps can be explained as follows. When the M-I-M structure is biased, electrons are stored in the trapping sites. These traps discharge when voltage is removed, but not as quickly as the electrodes to which the potential was applied. Using a sensitive electrometer, discharge currents can be seen with typical films for as long as several hours after the electrodes are shorted. Trapping also causes I-V hysteresis.[11] An I-V plot showing hysteresis in which the sample voltage was swept at a constant rate is given in Fig. 8.

The capacitance of M-I-M structures can be as high as 1 $\mu fd/cm^2$. Therefore, I-V hysteresis measurements must include a consideration of

the charging currents of the electrodes. The effects of simple capacitance and hysteresis were avoided by using very slow sweep rates in obtaining the data presented here.

The Biased M-I-M Structure--Tunneling Currents

Tunneling is a quantum-mechanical phenomenon whereby electrons may penetrate a classically forbidden barrier (the insulator in M-I-M structures) if the barrier is sufficiently thin.[12] There must be empty allowed states on the other side of the energy barrier at the same energy level as the filled states in order to achieve net tunneling currents.

There are two models with their resulting equations to describe tunneling in the "thin" and "thick" regimes. The models are shown in Figs. 10 and 11. The first equation is an approximate relation for direct tunneling given by Lindmayer and Wrigley.[3]

$$J \sim \frac{q\phi}{2\pi h d^2} \{\exp[-(4\pi d/h)(2m_e)^{1/2}(\phi - qV_a/2)^{1/2}] - \exp[-(4\pi d/h)(2m_e)^{1/2}(\phi + qV_a)^{1/2}]\}$$

These direct tunneling currents are usually negligible at thicknesses above 50 Å.

The strong thickness dependence of the direct tunneling current causes great difficulty when comparing theoretical and experimental I-V relations. Both the deposition and the thickness measurement of insulating films 10 Å - 50 Å thick are extremely difficult. Figure 12 shows some predicted direct tunneling resistivities taken from an approximate theory.[2] Figure 13 shows the resistance of experimental samples compared with the same theory.

The Fowler-Nordheim relation describes the currents predicted by the scheme shown in Fig. 11 and is given by[3]

$$J = J_o (E/E_o)^2 \exp(-E_o/E)$$

where $J_o \simeq 16\pi q\phi^2 m_e/9h$

$E_o = 8\pi\phi^{3/2}(2m_e)^{1/2}/3hq$

$E = V_a/d$

This relation predicts that tunneling may dominate the conduction current even in thick insulators because electrons can see a reduced barrier thickness at high biases, as the figure shows.[3,13] SiO_2 is reported to be an ideal insulator for studying Fowler-Nordheim tunneling because it can be prepared by the thermal oxidation of silicon.[14,15] SiO_2 prepared this way shows a remarkable absence of electron trapping effects.[14]

The Biased M-I-M Structure--Schottky Emission Currents

Schottky emission occurs when the electrons surmount the interfacial barrier, ϕ. Following Hartman, Blair, and Bauer,[16] a current flow which increases exponentially with the square root of the applied voltage for large fields is usually ascribed to Schottky emission. The Schottky emission equation modified for emission into an insulating film is given by[17,18]

$$J = \Lambda T^2 \exp(\delta V^{1/2} - \phi/KT)$$

where $\Lambda = 120\ A/(cm\text{-}K^o)^2$ is the Richardson constant, and

$$\delta = (q^3/\varepsilon\varepsilon_o d)^{1/2}/KT$$

Schottky emission may be the injection mechanism for space-charge-limited currents, in which case a space-charge-limited relation would

describe the resulting I-V characteristics rather than the relation above. For those cases in insulators where Schottky emission currents dominate the I-V characteristics, the possibility exists that under higher biases Fowler-Nordheim tunneling may replace Schottky emission as the dominant injection process.[19,20]

The Biased M-I-M Structure--Breakdown

Under high biases insulators show nonlinear I-V characteristics, and destructive breakdown is observed at 10^6 to 10^7 volts/cm. Budenstein, discussing breakdown conduction in thin films of SiO, MgF_2, CaF_2, CeF_3, CeO_2, and Teflon,* feels that breakdown is not a function of the pre-breakdown I-V-T characteristics. He goes on to discuss what he has physically observed when breakdown does occur:

> The measurements of the characteristics of single breakdowns wherein the voltage waveforms are correlated with the light intensity waveforms of individual spectral lines during breakdown are believed to provide a new perspective to the understanding of breakdown conduction. Based upon these, the optical micrography and the electrical measurements, a model of the many aspects of breakdown has been proposed. This represents an advance on a model previously suggested by the authors. The central feature in this model is the transition in a time of less than 10 nanoseconds from the pre-breakdown conducting state to a breakdown conducting state. In this time a region about 10 microns in diameter is converted from a solid into a conducting plasma. This conducting plasma is responsible for the low resistance during breakdown, for the light emission during breakdown, and for the final quenching of the breakdown.[21]

Low Bias Thick Film and Bulk Resistivity Description

Currents which appear to be linear with bias are observed in thicker (>25 micron) M-I-M structures, provided the steady current is low enough to avoid any significant modulation of conductivity by the injected carriers.[22] Therefore, a constant bulk resistivity

*Registered trademark, Dupont, Inc.

characterizes their conduction properties. The bulk resistivity depends upon the purity and structure of the insulator. For vacuum deposited films, the bulk resistivity is generally lower than for high quality, grown insulators.

The Stability of Insulators

The considerations discussed so far have been true in general for polycrystalline insulators. While most insulators are considered stable compounds, they exhibit distinct changes due to the ambient, and these changes can be detrimental during storage and long term usage. Similar changes could result from the effects of residual gas during vacuum deposition. Some data are given in the tables based on variation of I-V curves of samples for the insulators reported in this work. Many considerations of stability are very subtle and the evaluations given are only qualitative.

Long term adherence is an important thin film consideration which all the insulators used in this work passed. It must be mentioned again, however, that the evaporations were done onto aluminum electrodes. Vacuum conditions, substrate cleanliness, substrate material, and insulator thickness strongly affect adherence.

Forming Curves

The freshly prepared structures were not stable under the initial application of voltage. Sudden sharp changes in I-V characteristics were observed, usually at field strengths of 10^4 to 10^7 volts/cm. These irreversible changes are called "forming." In this work the forming generally resulted in decreased resistivities and more stable characteristics. There were, however, several cases of increased resistivities and additional forming during the second or third voltage ramp applied

to the structures. Figures 14 and 15, plotted on linear coordinates, show the inconsistent forming and the more consistent sweeps #3 and #4 after forming. Figures 16 and 17 show forming curves and breakdown for some of the M-I-M structures. Figure 18 shows the more consistent I-V curves for three samples after forming.

CHAPTER II

DESCRIPTION OF EXPERIMENTS AND EQUIPMENT

For the samples in this report a thin aluminum strip was vacuum evaporated onto a cleaned glass slide. The insulator was evaporated onto the aluminum and a counterelectrode deposited over the insulator.

All slides were precleaned using the following technique:

1. Scrub in Sparkleen.*
2. Rinse thoroughly in running distilled water.
3. Rinse in Sparkleen.
4. Rinse thoroughly in running distilled water.
5. Dry immediately with heat gun or filtered high pressure air.

The slides fogged uniformly under hot breath and 50-100 Å films of lead sulfide deposited uniformly on them. More thorough cleaning techniques developed using radioactive tracers have been reported in the literature.[23]

It is believed that glass slides are quite free from lapping and cutting oils which are found on semiconductor crystals and that this makes possible a different cleaning procedure. Glass is also much smoother than the surface of a semiconductor. Even after etching, the ratio of the surface of a 200 Å film of aluminum on glass to the geometric area is as low as 2.5.[23] This ratio is called the surface roughness factor. It should be as low as possible to achieve an insulator overlay with a high breakdown strength. Rhodium on glass has a roughness factor of nine. Often, annealing or exposure to reactive gases will reduce the true surface area considerably.[23]

Cleaved crystals will have a high surface roughness factor unless

---

*Fisher Scientific Co., 1458 N. Laymon Ave., Chicago, Illinois.

the cleavage occurs along a single crystallographic direction.

In a multilayer structure surface roughness will propagate through at least three interfaces, although there will be smoothing effects as the films are made thicker.[23]

Geometry of Samples

All samples were deposited on Lapine* Clinac selected microscope slides, which are soda-lime glass. A set of three masks was used; they could be changed only by opening the vacuum system. The first mask was used to deposit an aluminum base electrode 40 mm long and 1 mm wide onto the glass. The aperture in the second mask was 35 mm long and 3 mm wide. The insulator was deposited through this mask over the base electrode, except at the ends. The third mask formed nine counter-electrodes, which were approximately 10 mm long and alternately 1 or 2 mm wide, and at right angles to the base electrode. The samples were thus M-I-M capacitor structures. The areas of the samples were alternately 2 mm^2 or 1 mm^2.

The Choice of Electrodes

Nine Au-SiO_x-Au, nine Cu-SiO_x-Cu, and eight Pb-SiO_x-Pb structures were deposited to compare with Al-SiO_x-Al. The SiO_x was 200 Å thick on each structure. For the gold, lead, and copper structures a resistance of 10-30 Ω was measured. For the structures using aluminum electrodes, eight read between 10^9 and 10^{10} Ω. Ten ohms were measured on the ninth structure because no insulator was deposited in order to check the contact resistance, and for effects of oxide growth on the lower aluminum electrode. On at least one M-I-M structure for each

*Lapine Scientific Co., 6001 S. Knox Ave., Chicago 29, Illinois.

insulator, the insulator deposition was omitted. These metal-metal resistances always read 10 to 30 Ω. First breakdowns occurred on the Al-SiO_x-Al structures at 12 to 14 volts, with a large number of breakdown pulses at 14 to 16 volts.

A second set of tests was made. Eight Al-SiO_x-Au and eight Al-SiO_x-Pb structures were made to compare yields with Al-SiO_x-Al structures. The gold and lead were deposited on top of the insulator as counterelectrodes. All samples show similar resistances in the multimegohm range. The structures with dissimilar electrodes showed up to a factor of four resistance change with polarity. The Al-SiO_x-Al structures showed less than 5% resistance change with polarity.

It was concluded from the above that aluminum permitted deposition of the most uniform insulator overlay. The reason for this may be the monolayer of aluminum oxide which forms on the electrode, creating a "nest" for the insulator deposition. It was observed that when deposited on copper, gold, and lead electrodes, the insulators contained "voids" or "pinholes." M-I-M structures using gold and copper electrodes were unshorted when the SiO_x was deposited more than 500 Å thick. However, these structures had much lower breakdown voltages than similar structures using aluminum electrodes.

Description of the Vacuum System

An ordinary diffusion pumped vacuum system is shown schematically in Fig. 19.[24]

The vacuum system used in this work was a Carl Hermann and Associates* (CHA) system (Fig. 20) which was equipped with a Granville-Phillips**

---
*CHA Industries, Palo Alto, California.

** Granville-Phillips Co., 5675 E. Arapahoe Ave., Boulder, Colorado.

10 liter liquid nitrogen cold trap. The bell jar measured 18 by 30 inches. The system was equipped with a 12-hole baseplate and a 9-hole collar, giving good flexibility for the installation of hardware. Figure 21 shows the geometry of the installed hardware. The filament grounding strap was designed for this experiment along with the multiple source installation. The figure shows from left to right, a high voltage glow discharge feedthrough, a micrometer leak valve, the MRC electron beam gun, a water cooling feedthrough, a Drumheller source, and five tungsten or molybdenum boats.

The controls of the system shown in Fig. 20 include electro-pneumatic valves, two thermocouple (TC) gauges, two ionization gauges, and an automatic pumpdown-sequencing unit. The sequencing unit contains a TC gauge output meter-relay which closes when a preset pressure is reached during roughing. The roughing valve is then closed and the forepump and gate valves are opened through relays in the unit. For venting and starting there are two buttons and during automatic operation these are the only two necessary for pumpdown control. During venting the sequencing unit closes the gate valve and opens the vent until the operator releases the stop-vent button. The system need not be attended for switching from roughing to high vacuum operation. However, a gate valve should not be left open for long periods because after the liquid nitrogen trap warms up, oil vapor would enter the bell jar.

Figure 20 shows the deposition equipment installed in the bell jar. The sources were installed near the baseplate. The quartz crystal monitor and substrate were located above at a distance of 20 to 60 cm from the sources. For very thin (<300 Å) insulator depositions "geometric leverage" was used to increase the deposition on the crystal.

Several evaporations used the crystal at 30 cm and the substrate at 60 cm from the source. The monitor then read four times the actual deposition thickness. If the crystal is located too close to the source, it may tend to stop oscillating if the radiative heating is excessive.

The materials which were vacuum deposited were placed in a group of evaporation sources as shown in Fig. 21. The high current feedthroughs were fed to a five-position switch. A change of source required merely rotating the source selector switch. Differing materials were never evaporated from the same source to avoid contamination of the deposited film. Pyrex shields used over each source not only prevented cross-contamination, but aided in keeping the bell jar and baseplate clean.

Deposition Methods Used

Thermal evaporation is achieved by raising the temperature of the material in a vacuum system until its vapor pressure is appreciable, i.e., at least 10^{-3} Torr. The system vacuum must be much better than that to reduce contamination, i.e., 10^{-6} Torr. In this pressure range there is little chance for collision of the escaping molecules with residual gas in the system. When the molecules strike a surface they will stick or be reflected. The sticking coefficient may be close to unity depending on the evaporant, the substrate, and the cleanliness of the substrate. The residual gas can also be built into the film. A background pressure of 10^{-6} Torr corresponds to an arrival rate for the residual gas of about one monolayer per second.

For the insulators in this experiment two evaporation methods were used: direct heating and electron bombardment. Direct heating required installation of a resistance source; tungsten and molybdenum boats, filaments, and tungsten heated ceramic crucibles were used. The sources

are constructed to operate at 5 to 10 volts with a current of 40 to 200 A. No attempt was made to choose the optimum source as too few evaporations of any insulator except SiO_x were made, for which the Drumheller* source is standard.

Electron bombardment was achieved with an MRC** electron beam deposition unit powered by a Varian† 2kW beam deposition power supply. The principle of electron beam deposition is similar to that of a simple vacuum diode. A negative 4 kV bias is applied to a filament electron source. The electrons are accelerated through the 4 kV potential, striking the grounded anode containing the evaporant. The hearth itself is water cooled but the material, being in the electron path, is heated by absorbing energy from the electrons. The construction of the power supply requires that filament temperature be controllable. It also requires self-protection from arcing which is a frequent occurrence even in normal operation. A sustained arc can form between the filament and cup in the deposition unit, causing a very high surge current which could damage the power supply. Two features of the Varian supply prevented any damage: a saturable transformer with suitable high voltage insulation and an overcurrent-cutoff interlock. Two additional interlocks insuring adequate water flow and a closed bell jar were used with the electron beam equipment. A water flow of 0.25 G.P.M. was maintained to carry off up to 2 kW of heat developed at the cup. The bell jar interlock protects the operator from possible contact with the high voltage inside the system.

---

*Drumheller source: Allen Jones Corp., Gardena, California.
**Materials Research Corp., Orangeburg, New York.
†Varian Associates, Palo Alto, California.

Thickness Monitors

Four methods were used to determine film thickness. The first two were possible only after deposition. The first used weight determined by a microbalance plus area and evaporant density. This is primarily a calibration technique. The second observed the step at the edge of the film via an interference microscope. These two methods are limited to films thicker than about 500 Å. The second two were monitoring methods used during deposition to prepare evaporated films of specified thickness.

A Sloan* Deposit Thickness Monitor (DTM) included an oscillator head with an attached, exposed, 5 mHz quartz crystal. The crystal was inserted into the vacuum system beside the substrate. As deposition proceeded, the mass of the quartz crystal increased, causing the crystal's resonant frequency to decrease. This frequency change was compared to a heterodyne VFO in the control box and the difference frequency was shown on a panel meter. A simple formula, thickness $\simeq 2\Delta f/\rho$,[25] where ρ is the density (ρ = resistivity elsewhere in this report) of the evaporated material, converts the frequency change to thickness. The "2" in this formula is best regarded as a constant to be determined empirically.

There were several technological difficulties encountered with the Sloan DTM:

1. When dielectrics are evaporated, the spring crystal contact to the metallized surface of the quartz slab may become insulated from the crystal, and oscillation will cease.

2. When extremely high surge voltages are present during discharge cleaning or electron beam evaporation, transients may be induced. The

---

*Sloan Instrument Corp., Santa Barbara, California.

sparking caused at least one oscillator unit to fail. (An electrostatic shield was used subsequently to prevent this.)

3. Heating of the crystal caused its frequency to drift and necessitated either water cooling of its mount or a time delay between evaporation and reading of the frequency change. A water cooled crystal holder is marketed by Sloan. Water cooling tubes make it difficult to change the crystal location in the vacuum system.

4. Vacuum compatible insulated wire should be used to couple the oscillator to the vacuum system feedthrough. Single conductor No. 26 AWG Teflon coated wire was used for most work. All connections were crimped, not soldered.

The crystal monitor gave some trouble even at greater distances when used with the electron beam unit. A final thickness reading sometimes had to be obtained by waiting a few minutes after deposition to take final readings. Electrons from the gun travel to all parts of the bell jar. This was easily observed by sprinkling 5% europium doped gadolidium oxide[26] powder on the metal parts of the vacuum system and observing the red cathode luminescence which appeared when the beam unit was turned on. The powder was easily removed from the system after the test with a vacuum cleaner. It is felt that the electrons, in addition to the heat, can be detrimental to the stable operation of the crystal circuit. While no monitoring method is superior in all respects, quartz crystal monitoring was used because it was adequate, simple, and convenient for these depositions.

Dual ionization guage thickness monitoring was used for several early evaporations. One ionization guage was placed in the vapor stream, and the other, shielded from the stream, was nearby. The vapor stream caused a local pressure increase proportional to evaporant density.

The gauge currents were fed to a differential electrometer, the difference in current being calibrated to yield evaporation rate.

Both monitoring methods lend themselves through the use of feedback to evaporation rate control. The ionization gauge monitors were used to control rate between 0.1 Å/sec and 100 Å/sec during evaporation of gold films on glass substrates. The rate was kept constant within a few per cent. Rate control was tried with silicon monoxide, but the results were erratic. A calibration could not be made that remained valid and the rate sometimes slowly increased during evaporation. This may have been caused by the dielectric evaporant coating the collector and grid of the ion gauge and reducing the current.

The original gauges broke several times because they were too fragile to be installed, positioned, and removed frequently from the vacuum system. On the basis of these results, more rugged gauges were designed.* The new gauges featured elements isolated from the vapor stream so that results with insulators were improved with regard to consistency and accuracy.

A 100 kHz capacitance bridge was used with a few films to verify thickness after removal from the system. The disadvantage of this method is that the dielectric constant is known to vary depending on evaporation conditions. Thickness was calculated from the formula, $C = \varepsilon\varepsilon_o A/d$. This formula neglects potential penetration into the electrodes and thus d is in slight error. Ku and Ullman discuss the need to consider this effect, especially for very thin dielectrics and low density metals.[27]

---

*Mr. Jon Culton and Mr. Dale Coad were responsible for the design and construction of the improved gauges.

Decomposition

Since most materials used for insulating films are compounds, the possibility of decomposition on heating exists. If the material decomposes, its vacuum deposition will become difficult, if not impossible. The binding energy of the atoms in the molecule should be much greater than the cohesive energy of the crystal. Because decomposition will occur at thermal energies far below the interatomic binding energy, decomposition can be observed in many cases during deposition. Metal oxides which decompose leave the elemental metal deposited on vacuum system surfaces. Other symptoms may be a color change (not related to interference) and semiconducting rather than insulating properties in the resulting film.

Evaporation of $ThOF_2$

Comparisons of thickness measurements on $ThOF_2$[28] indicated there may be inconsistencies. Also the $ThOF_2$ residue in the source became more difficult to evaporate as the charge was used. It is likely that the deposited films were actually ThF_4 and the residue in the source ThO_2.[19] Therefore, the data obtained would be data for ThF_4 films. Heitmann and Ritter reported ThF_4 films to be amorphous and highly etch resistant.[19] The evaporated films are highly transparent also, and might be tried for passivation of luminescent devices. Thorium compounds are radioactive and aluminum foil liners in the apparatus and the wearing of a respirator for cleaning are recommended by the above authors.

Types of Measurements

The samples were measured in several tests. Breakdown field strengths were compared to published data when available. This was

done by applying voltage until destructive burnout occurred and recording the critical electric field. Most of the samples broke down, as may be seen from the data, at field strengths of 10^6 to 10^7 volts/cm. This along with high low-voltage resistance is sufficient to assure freedom from pinholes. A pinhole will breakdown at from 2 to 5 x 10^4 volts/cm. A metal to metal short as small as 30 Å will appear to be a short circuit. If one or two monolayers of oxide ($\approx$10 Å) were to form between subsequent depositions of electrodes, the short resistance would not be affected. This can be verified by observing from Fig. 12 that tunneling resistance would be less than one ohm, compared to lead resistance in the order of 10 ohms.

Low-voltage resistances were read using a four point technique. The linear coordinate I-V curves and breakdown voltages were recorded on an X-Y plotter. The semilog plots were obtained using one Keithley* 600 A electrometer to indicate voltage and another for current. Voltage was applied using a regulated dc power supply.

Because of the nonlinear nature of the sample resistances, a fixed one volt was applied and the resultant steady current recorded. Resistance scales can give misleading results because the electrode voltage varies with the scale chosen. It is very likely that the one volt applied in some cases did modulate the sample conductivity and was therefore not a true bulk resistivity reading; however, applied voltages less than one volt cause currents so small as to require difficult sample shielding techniques. This was not attempted because of the large number of M-I-M structures made and evaluated.

For most of the films, ε was calculated from the measured capaci-

---

*Keithley Instrument Corp., 12415 Euclid Ave., Cleveland, Ohio.

tance and listed in the data section. The values of d were those measured with an interferometer. Higher than expected dielectric constants were observed. This may be due to the high frequency (100 kHz), the strong trapping effects, and electrode effects.[27] The data were sparse and no error analysis was attempted for the relative dielectric constants.

Self-Healing Breakdown Technique of Measuring Maximum Voltages and Pinholes

A technique reported by Klein and Gafri[29] for looking at the maximum breakdown strengths of insulators was tried. The aluminum counterelectrode is made less than 1000 Å thick. When breakdown occurs, the discharge burns back the electrode instead of letting it melt through to form a short. The voltage can then be increased again. The location of a burnout is observed through a microscope. Thus, the capacitor has "self-healed" and revealed the location of its weak spots and their number. From these tests film uniformity can be determined. On one sample breakdown occurred at 3V, 4V, 10V, 15V, and 18V before destructive breakdown occurred. The early breakdowns were observed to be along the perimeter of the M-I-M structure. This same observation is reported by other experimenters.[20]

Breakdowns near burnout slowly propagated on some structures, forming irregular lines that wandered through the sample. Popping sounds were audible. Observation was through an optical microscope, using 80x mignification and backlighting. Thirty to 100 distinct burnout holes could be seen in some structures before destruction. In addition, the initially smooth electrodes became rough and dull in appearance over the active region.

It is felt that this technique served the very useful purpose of determining uniformity of thickness of insulators in M-I-M structures.

Particularly, this technique was used to determine that insulators formed more uniformly on aluminum than on gold, copper, or lead.

Comparison of Electron Beam and Filament Evaporation

The electron beam technique does not show overall superiority to filamentary evaporation. It can do a wider variety of materials and larger volumes in shorter times. The higher initial cost and occasional arcing problem, which renders all ionization gauges in the system inoperative, are its major disadvantages. The film adherence, pinhole density, and ease of use seemed reasonably similar for both methods for the insulators tested. The hearth in the beam gun will far outlast filament sources and frequent use of one or two materials can pay the cost of the beam unit in filament replacement costs alone. For the high temperature oxides and metals the beam unit shows its superiority both by ease of evaporation and by keeping the vacuum system and substrate cooler. Spitting, if it is a problem, as with silicon monoxide, was a problem with both the beam and filament. A Drumheller type source as a filament and proper material form were solutions to this problem.

The MRC direct beam unit functioned well with the Varian power supply. The electron beam unit and filament sources were found to complement one another for the materials in this work. Due to long hearth and filament life, the beam unit has an advantage with respect to servicing. However, the charge must be carefully placed in the hearth to prevent its jumping out during evaporation.

Conclusions and Data

The prime aim of this work was to characterize electrical properties of some vacuum deposited insulating films with the intent of determining

their suitability for device use. Available sources were both electron beam and resistance heated types.

The compiled and averaged data are given in the tables and supplemented with a few I-V curves. No thin film insulator was found to be superior to SiO_x evaporated from a Drumheller source. $ThOF_2$ is suggested for trial as a passivator where convenience and optical transparency are desirable. All the insulators tried, except for TiO (this was not TiO_2), could, under the proper means, yield acceptable, adhering, insulating films of 50% or higher yields when deposited on aluminum electrodes on glass microscope slides.

Table 1. Summary of Parameters

Thin Film Insulating Material[26,28,30]	SiO_x	Al_2O_3	MgO	MgF_2	CeO_2	CeF_3	$ThOF_2$	TiO	$(Gd_{.955},Eu_{.045})_2O_3$
Density[19,31,32]	2.1	3.4	3.8		7.1			4.9	7.4
Electron Beam Evaporable	Yes	Yes	Yes	Yes	Severe Arcing	Spits	May Form ThF_4 Films	De-composes	Spits
Filament Evaporable[a]	Drum-heller	No	No	Yes	No	No			Yes
Evaporation Temperature	Low	High	Medium	Low	Low	Low	Low	High	High
% Yield[b]	100	100	62	75	79	94	80	0	50
Peeling Thickness[c] (μM)	>4.0			2.2	.97	1.0	>2.5		.5
Resistivity for 1 Volt Applied (ave.) (ohms)	$>10^{12}$	10^{12}	10^{11}	10^{11}	10^{10}	10^{12}	10^{9}		10^{10}
Thickness[d] (Å)	500	700	225	420	160	700	275		1500
Breakdown[d] (V/cm x 10^{-6})	8	5	7	2	6	4	2		2
Comments	Best overall	2nd best by e^- beam		2nd best by filament			Most transparent		Lumines-cent

[a] Includes crucibles, Drumheller source, boats, or coil filaments.
[b] Using glass substrate and aluminum electrodes.
[c] Using room temperature glass slides, aluminum electrodes, and filament source.
[d] Dielectric breakdown strength for the thickness listed.

Table 2. Filament Evaporated Insulators ~300 Å thick.

Thin Film Insulating Material	SiO_x	Al_2O_3	MgO	MgF_2	CeO_2	CeF_3	$ThoF_2$	TiO
Forming Curve Number in Fig. 16 or Fig. 17				78-2	72-1			
Film Thickness by DTM (Å)	330		300					130
Film Thickness by Interferometer (Å)	250		195	867	159	475	281	140
Capacitance[a] (pF)			6300	663	2510		2600	
Dielectric Constant[b]			14	6.5	4.5		8.3	
D.C. Resistivity for 1 Volt Applied (ave) (ohm-cm)			$2x10^5$	$4x10^9$	$2x10^8$		$3.5x10^5$	$1.5x10^{10}$
Dissipation Resistivity[c]			$1.0x10^5$	$7.7x10^5$	$4.4x10^5$		$2.6x10^4$	
V_L First Breakdown (volts)	13		1	14			3	
V_h Destructive Breakdown (volts)	14			19	10		5	10
Comments	Drumheller source	Supports melted	Evidence of decomposition					Alumina basket melted

[a]Using a 100 kHz bridge.
[b]Sparse data - rough values; $\varepsilon = Cd/\varepsilon_o A$.
[c]As calculated from dissipation using a 100 kHz bridge.

Table 3. Electron Beam Deposited Insulators ~300 Å thick.

Thin Film Insulating Material	SiO_x	Al_2O_3	MgO	MgF_2	CeO_2	CeF_3	$ThOF_2$	TiO
Forming Curve Number in Fig. 16 or Fig. 17	52-4		53-4	56-3		59-6		
Film Thickness by DTM (Å)	360		300		100			100
Film Thickness by Interferometer (Å)	330	700	220	420		680	280	
Capacitance[a] (pF)		1120	2750	1240		1750	3730	
Dielectric Constant[b]		8.9	6.9	5.9		14	12	
D.C. Resistivity for 1 Volt Applied (ave) (ohm-cm)	$1.5x10^{11}$	$2.8x10^{12}$	$3.7x10^{10}$	$1.1x10^{12}$		$1.4x10^{12}$	$8.2x10^{8}$	
Dissipation Resistivity[c]	$4.5x10^{6}$	$1.9x10^{5}$	$4.4x10^{6}$	$5.2x10^{4}$		$2.9x10^{5}$	$1.1x10^{5}$	
V_L First Breakdown (volts)	6	16	9	5		16		
V_h Destructive Breakdown (volts)	28	35	16	10		25	1	
Comments			Carbon hearth used;outgases		All samples shorted	Spits		All samples shorted

[a]Using a 100 kHz bridge.
[b]Sparse data - rough values; $\varepsilon = Cd/\varepsilon_o A$.
[c]As calculated from dissipation using a 100 kHz bridge.

Table 4. Filament Evaporated Insulators ~5000 Å thick.

Thin Film Insulating Material	SiO_x	Al_2O_3	MgO	MgF_2	CeO_2	CeF_3	$ThOF_2$	TiO	$(Gd_{.955}, Eu_{.045})_2O_3$
Forming Curve Number in Fig. 16 or Fig. 17	65-4		67-4	79-3	73-4		66-4		
Film Thickness by DTM (Å)	5000						5000		
Film Thickness by Interferometer (Å)	6320		5360	8050	3100	5525	5530		1500
Capacitance[a] (pF)	167		81	254	532		190		991
Dielectric Constant[b]	12		5.0	23	19		12		17
D.C. Resistivity for 1 Volt Applied (ave) (ohm-cm)	1.5×10^{11}		1.8×10^{11}	1.2×10^{10}	4.0×10^{7}	1.8×10^{7}	3.9×10^{9}		2.7×10^{10}
Dissipation Resistivity[c]			4.9×10^{6}	1.9×10^{4}	3.9×10^{4}	0	1.1×10^{6}		9.3×10^{5}
V_L First Breakdown (volts)	>70			>70	>70		16		18
V_h Destructive Breakdown (volts)							20		33
Comments	Drumheller source	Supports melted	Evidence of decomposition					Decomposed	Powder spits

[a] Using a 100 kHz bridge.
[b] Sparse data - rough values; $\varepsilon = Cd/\varepsilon_o A$.
[c] As calculated from dissipation using a 100 kHz bridge.

Table 5. Electron Beam Deposited Insulators ~5000 Å thick.

Thin Film Insulating Material	SiO_x	Al_2O_3	MgO	MgF_2	CeO_2	CeF_3	$ThOF_2$	TiO
Forming Curve Number in Fig. 16 or Fig. 17	54-4	64-4	55-5	57-3	58-7	60-3	62-4	63-5
Film Thickness by DTM (Å)	2000	3540	2000				5000	1400
Film Thickness by Interferometer (Å)	1750	3000	1950	7580	2670	4570	12,500	2050
Capacitance[a] (pF)	535	221	543	312	680	290	190	830
Dielectric Constant[b]	11.6	7.5	12	27	21	15	27	19
D.C. Resistivity for 1 Volt Applied (ave) (ohm-cm)	2.3×10^{9}	3.3×10^{11}	7.3×10^{10}	3.3×10^{10}	3.1×10^{10}	7.3×10^{11}	1.6×10^{9}	4.9×10^{6}
Dissipation Resistivity[c]	8.5×10^{5}	3.3×10^{6}	5.1×10^{5}	2.4×10^{4}	1.2×10^{5}	3.3×10^{5}	8×10^{5}	4.9×10^{4}
V_L First Breakdown (volts)		770		33	29	45	15	
V_h Destructive Breakdown (volts)			71	>70	67	>73	30	14
Comments	Cu-color contamination		Carbon hearth used;outgases		Extreme arcing	Spits	Easy	Decomposed

[a] Using a 100 kHz bridge.
[b] Sparse data - rough values; $\varepsilon = Cd/\varepsilon_o A$.
[c] As calculated from dissipation using a 100 kHz bridge.

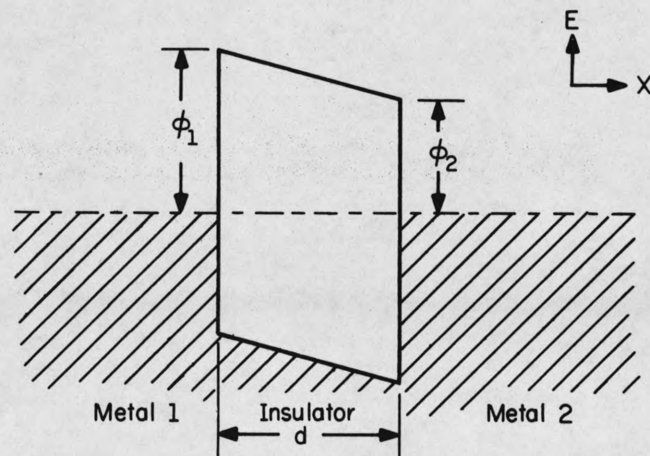

Figure 1. Energy band diagram of an M-I-M structure at zero bias, showing the heights of the insulator forbidden gap above the Fermi levels.

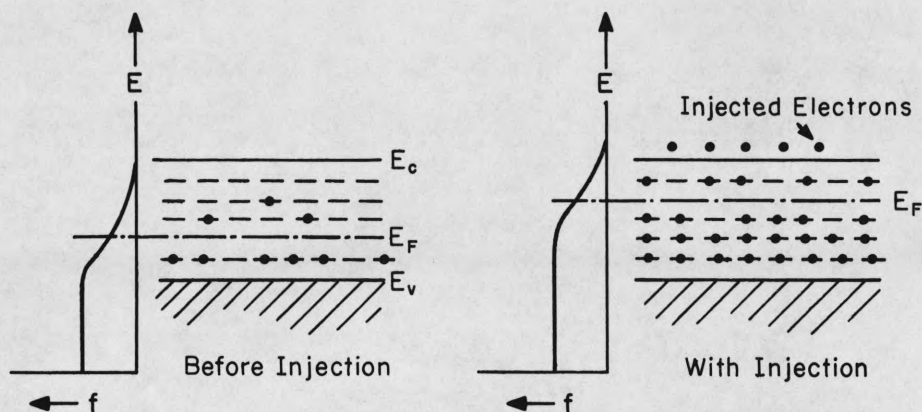

Figure 2. Energy band diagram of an insulator showing the increase in occupation of a continuum of trapping levels due to injected electrons.

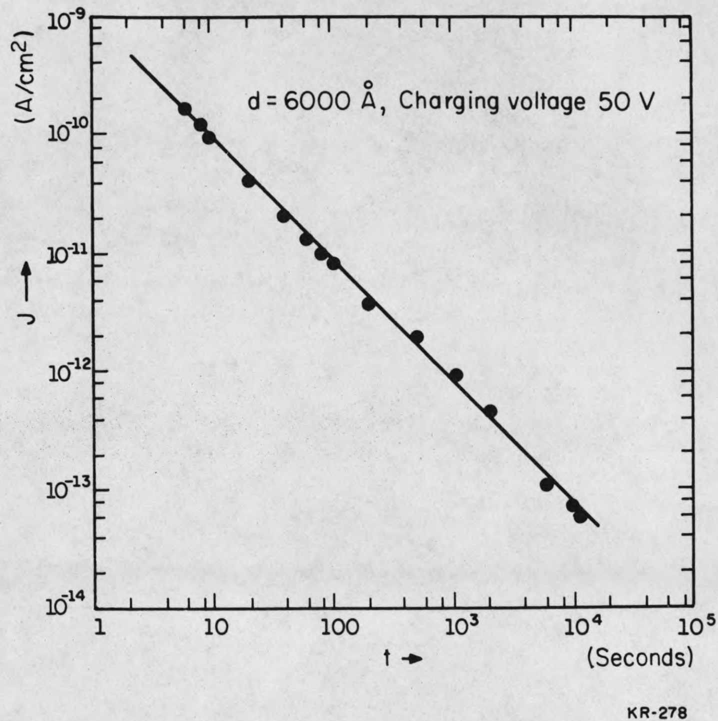

Figure 3. Experimental long-term discharge current from a Al-SiO_2-Si structure. The SiO_2 (6000 Å) was thermally grown. (From Lindmayer & Wrigley, Fundamentals of Semiconductor Devices, D. Van Nostrand Co., Princeton, N.J., 1964, p. 442.)

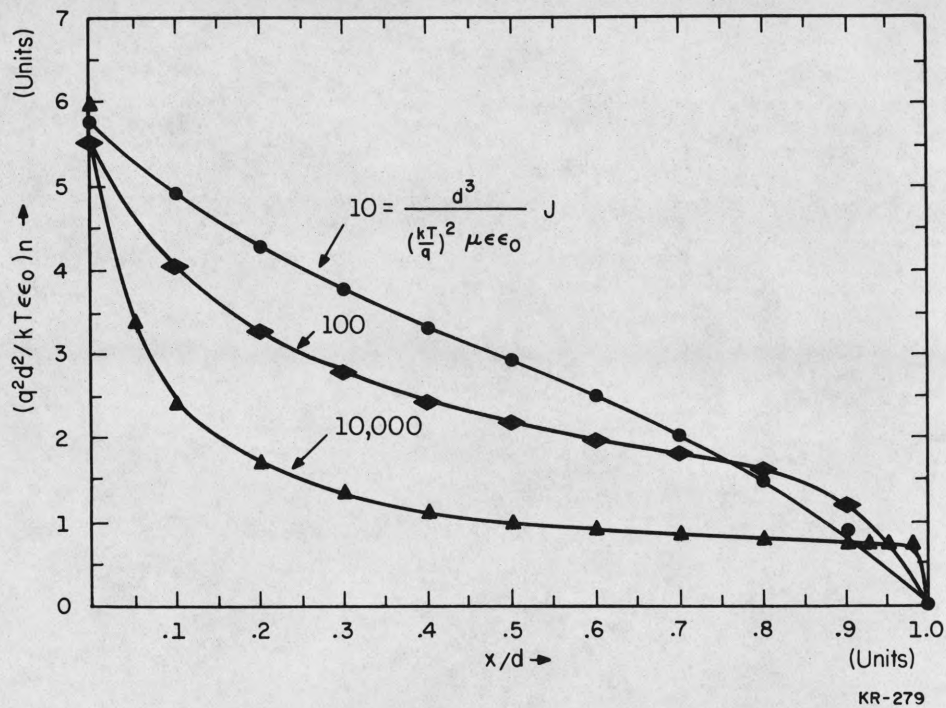

Figure 4. Best fit curve through computer generated points for the electron distribution in an insulator for one-carrier space-charge limited current. The ordinate applies to the normalized current of magnitude 10. For the normalized current of 100 the vertical scale should be multiplied by five, and by 100 for the normalized current of 10,000. (From Lindmayer & Wrigley, Fundamentals of Semiconductor Devices, p. 436.)

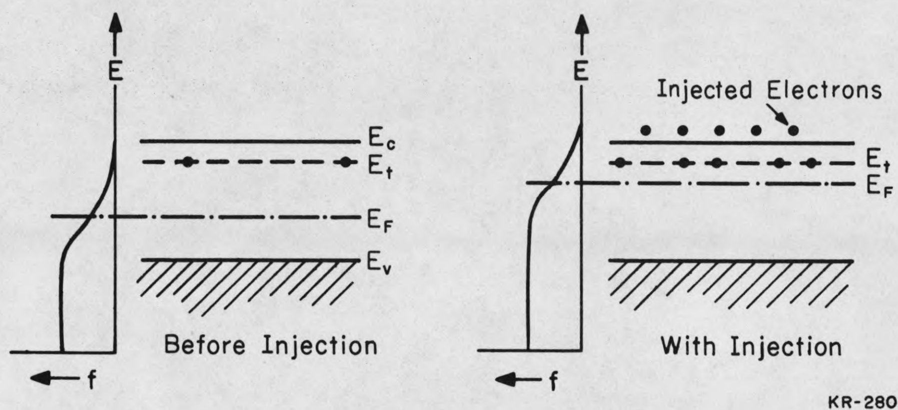

Figure 5. Energy diagram band of an insulator showing the increase in occupation of a single trapping level due to injected electrons.

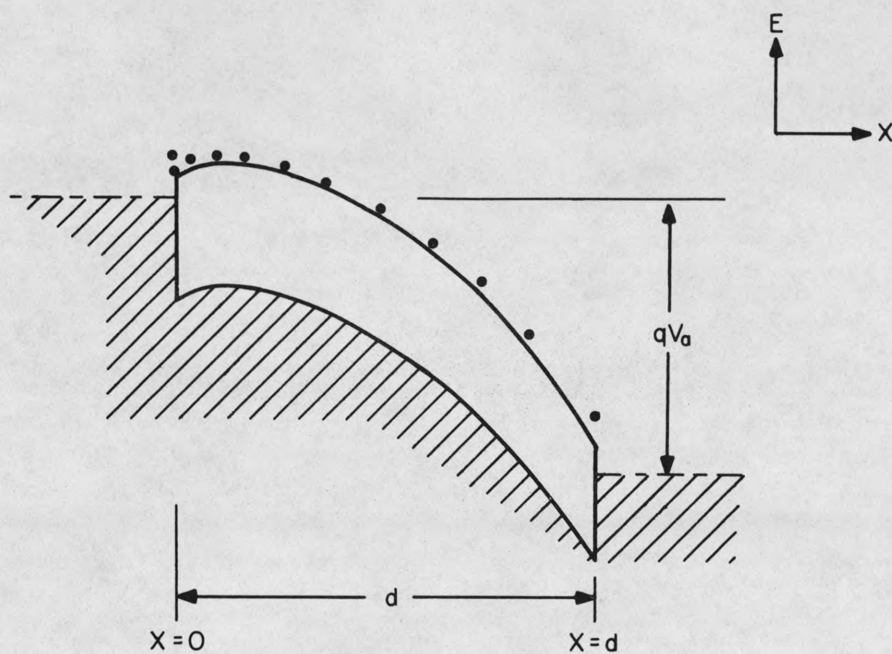

Figure 6. Energy band diagram for a biased M-I-M structure showing a single carrier (electron) space charge. An approximate relation for the current is $J = 9\varepsilon\varepsilon_o q V_a^2/8d^3$.

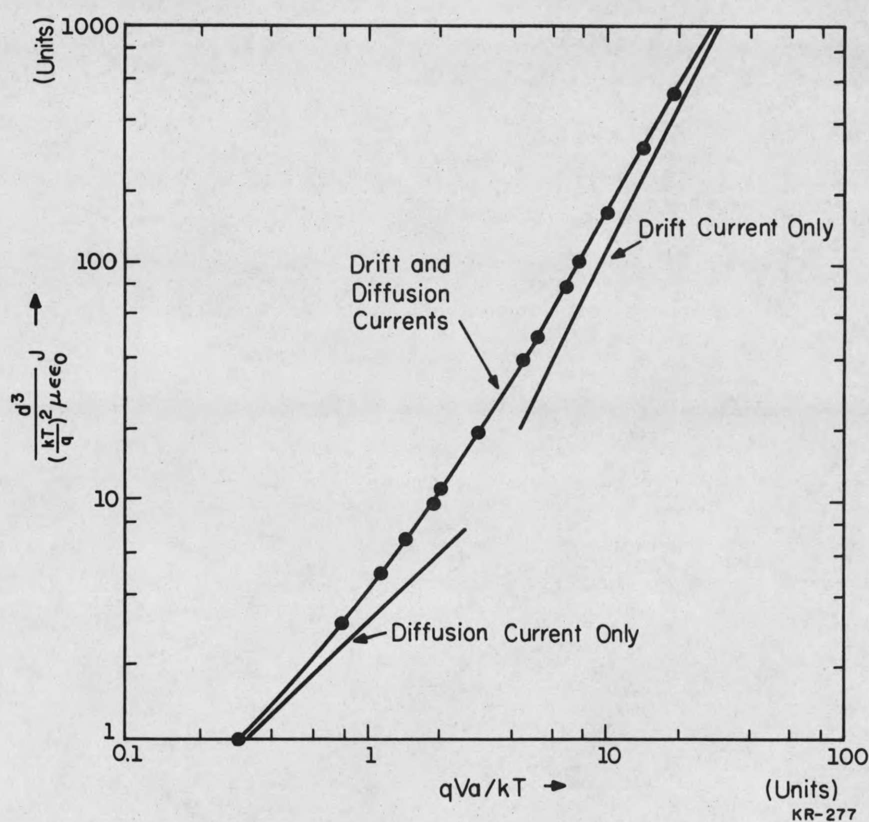

Figure 7. Best fit curve through computer generated points for the current-voltage relation for one-carrier space-charge limited current. For practical voltages the characteristic is quadratic. (From Lindmayer & Wrigley, <u>Fundamentals of Semiconductor Devices</u>, p. 435.)

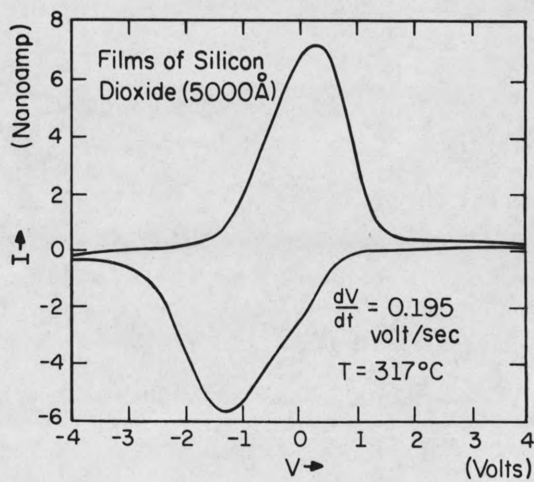

Figure 8. Current-voltage relation showing hysteresis in an Al-SiO_2-Si structure. The SiO_2 (5000 Å) was thermally grown. (From S. M. Hu, J. Electrochemical Soc. 113, 697 (1966).

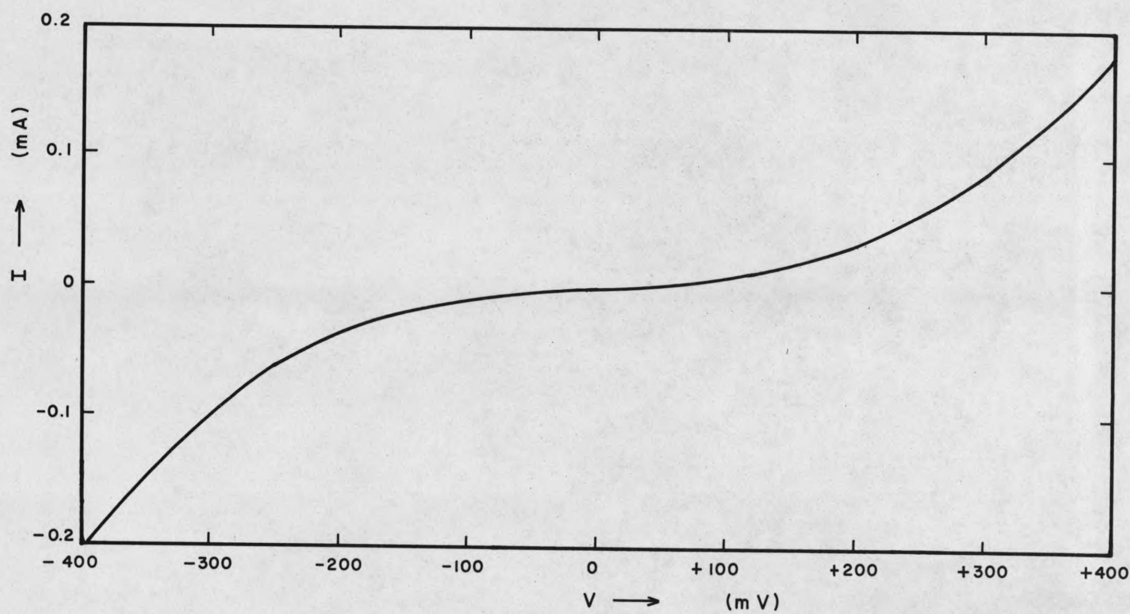

Figure 9. Slow sweep rate current-voltage relation for an Al-TiO-Al structure. The TiO (~100 Å) was electron beam deposited. Some decomposition probably occurred causing the extraordinarily low resistance. The current follows closely $J \propto V_a^2$ showing the space-charge-limited effect.

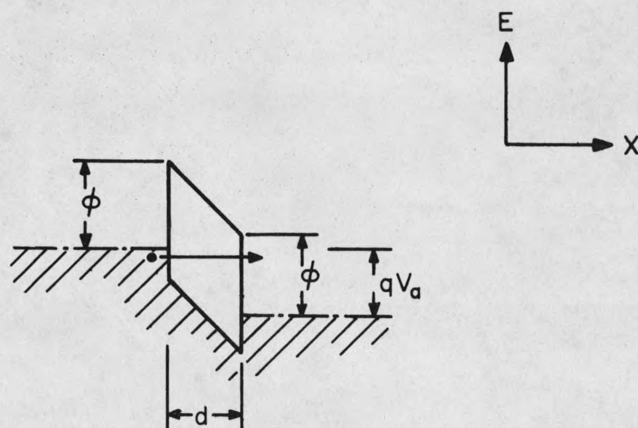

Figure 10. Energy band diagram for a biased M-I-M structure where the insulator is thin enough for the electrons to penetrate by direct quantum mechanical tunneling.

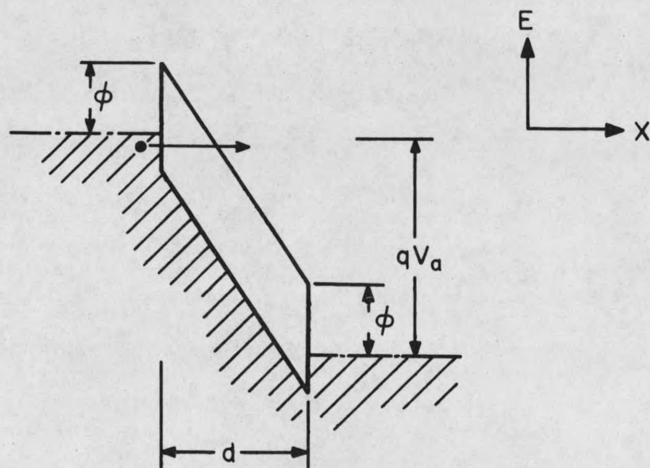

Figure 11. Energy band diagram for a biased M-I-M structure where the bias is great enough for the effective barrier thickness to be reduced. This leads to Fowler-Nordheim tunneling.

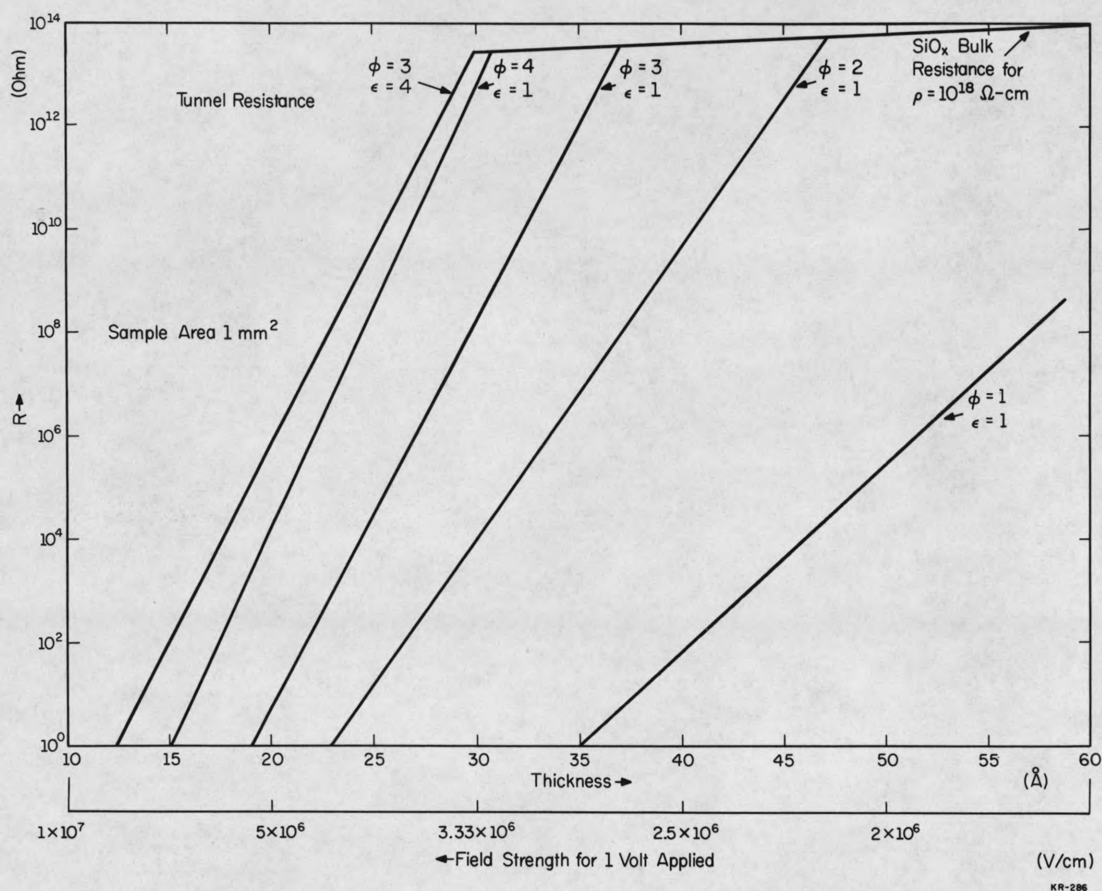

Figure 12. Low voltage theoretical tunnel resistance vs. thickness for various barriers corrected for image forces. SiO_x tunnel resistance has been plotted from estimates based on a barrier height ϕ = 3 and dielectric constant of 4. The range of experimental resistances for Al-SiO_x-Al structures is expected to lie to the right and below the SiO_x lines shown above. (From J. G. Simmons, J. Appl. Phys., <u>34</u>, 1802 (1963).)

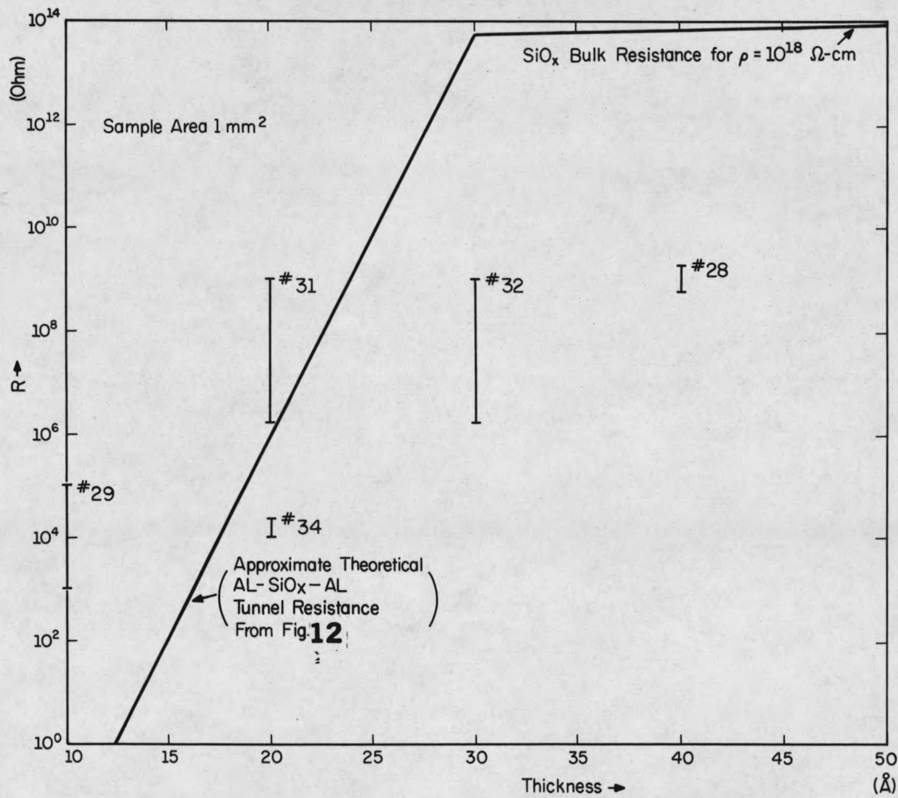

Figure 13 Low voltage resistance vs. thickness for 40 samples from five slides. For comparison the bulk resistance and tunnel resistance curves from Fig. 12 have been reproduced. Thickness was measured using a crystal monitor and "geometric leverage."

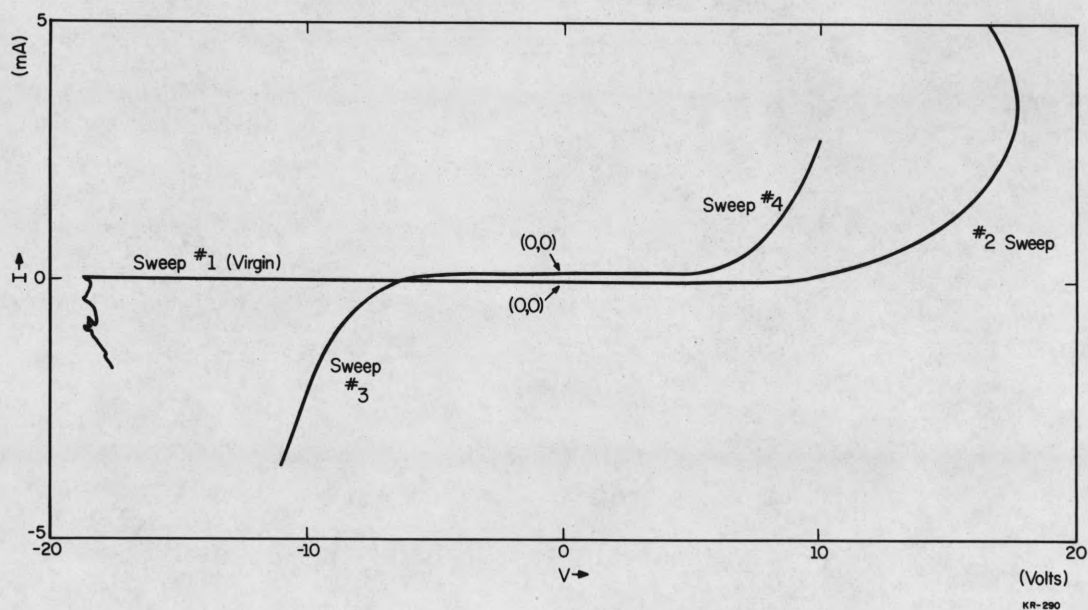

Figure 14 . Slow sweep rate current-voltage relation for an Al-$ThOF_2$-Al structure. The $ThOF_2$ (900 Å) was electron beam deposited. The negative resistance which appears here is a result of the forming and is non-repeatable. These results, taken on an X-Y plotter, are typical of the type obtained when applied fields are high enough to cause forming but not high enough to cause destructive breakdown. All four sweeps were started at the points marked (0,0) and are separated for clarity. For less than 5 volts applied, the current is in the nano-ampere range.

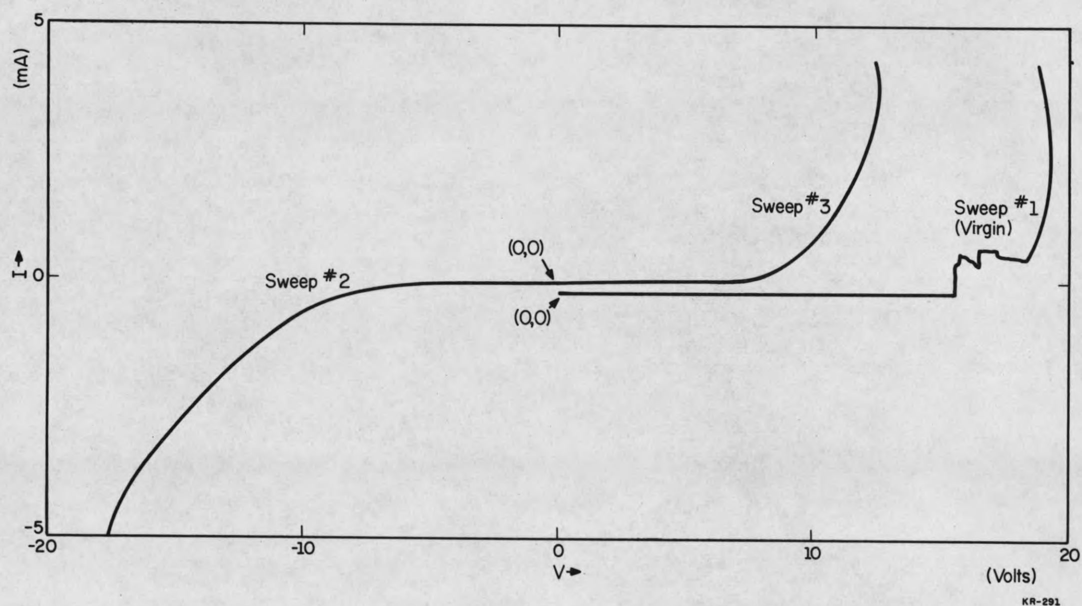

Figure 15. Slow sweep rate current-voltage relation for Al-$ThOF_2$-Al structure. The $ThOF_2$ (900 Å) was electron beam deposited. The negative resistance which appears here is a result of the forming and is non-repeatable. At lower currents than those resolvable on this curve the D.C. current-voltage relation after forming is repeatable. All three sweeps were started at the points marked (0,0).

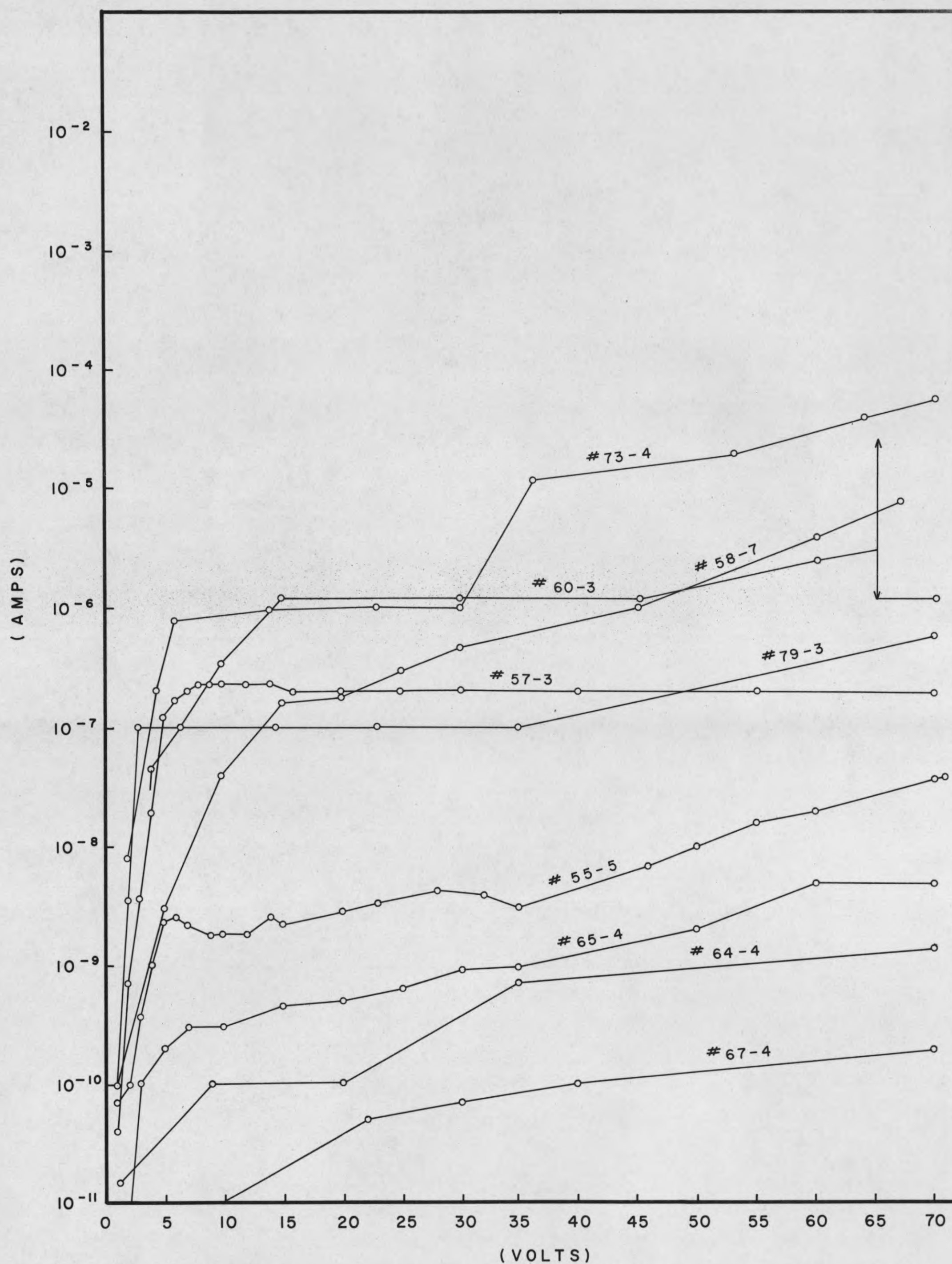

Figure 16. Al-Ins.-Al structure forming curves (first application of voltage) for vacuum deposited insulators. Breakdowns, when observed, are shown with arrowheads. The base electrode was deposited ≃1500 Å thick and the counterelectrode deposited ≃800 Å thick. See tables for information about each insulator.

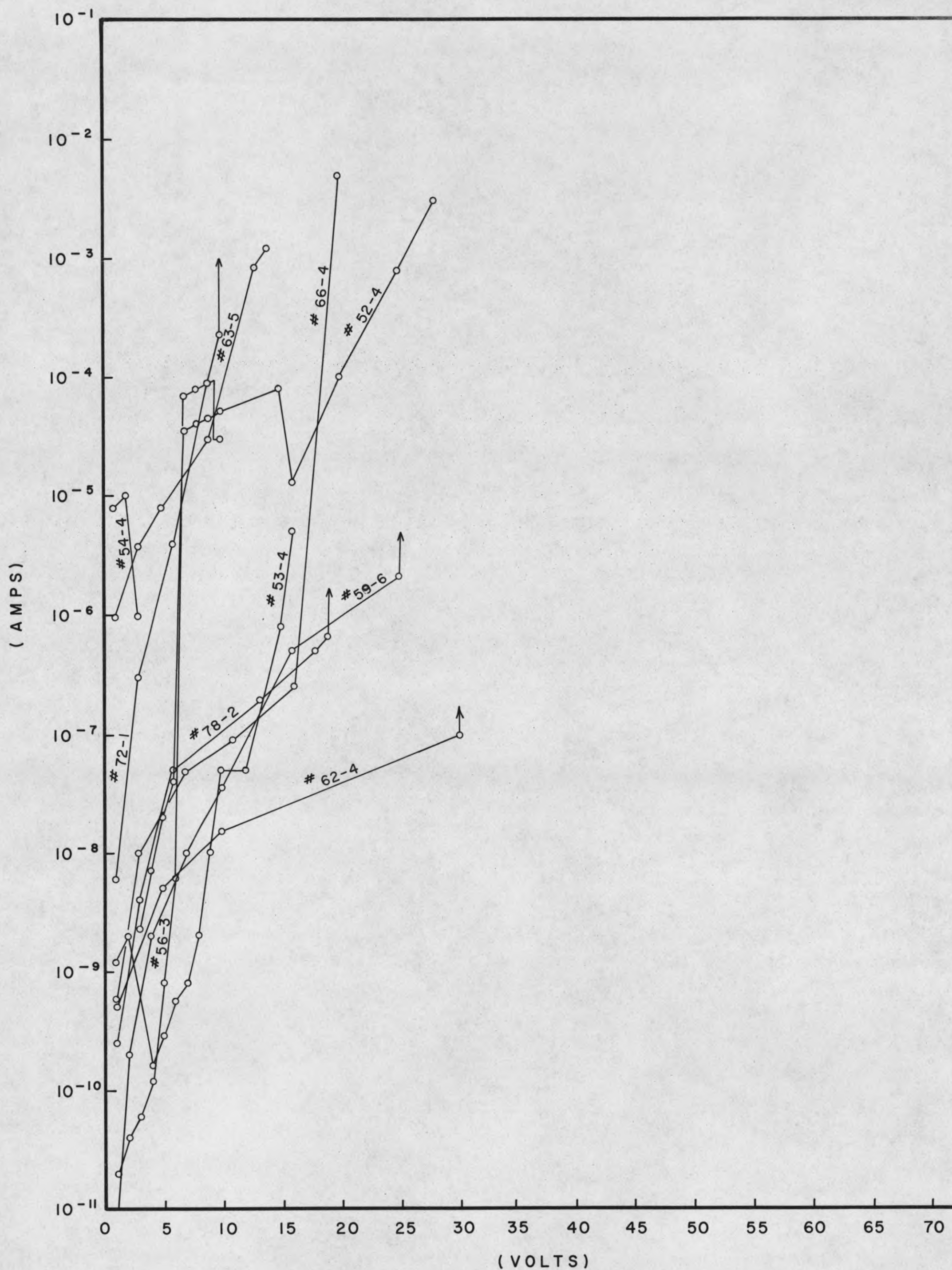

Figure 17. Al-Ins.-Al structure forming curves (first application of voltage) for vacuum deposited insulators. Breakdowns, when observed, are shown with arrowheads. The base electrode was deposited ≃1500 Å thick and the counterelectrode deposited ≃800 Å thick. See tables for information about each insulator.

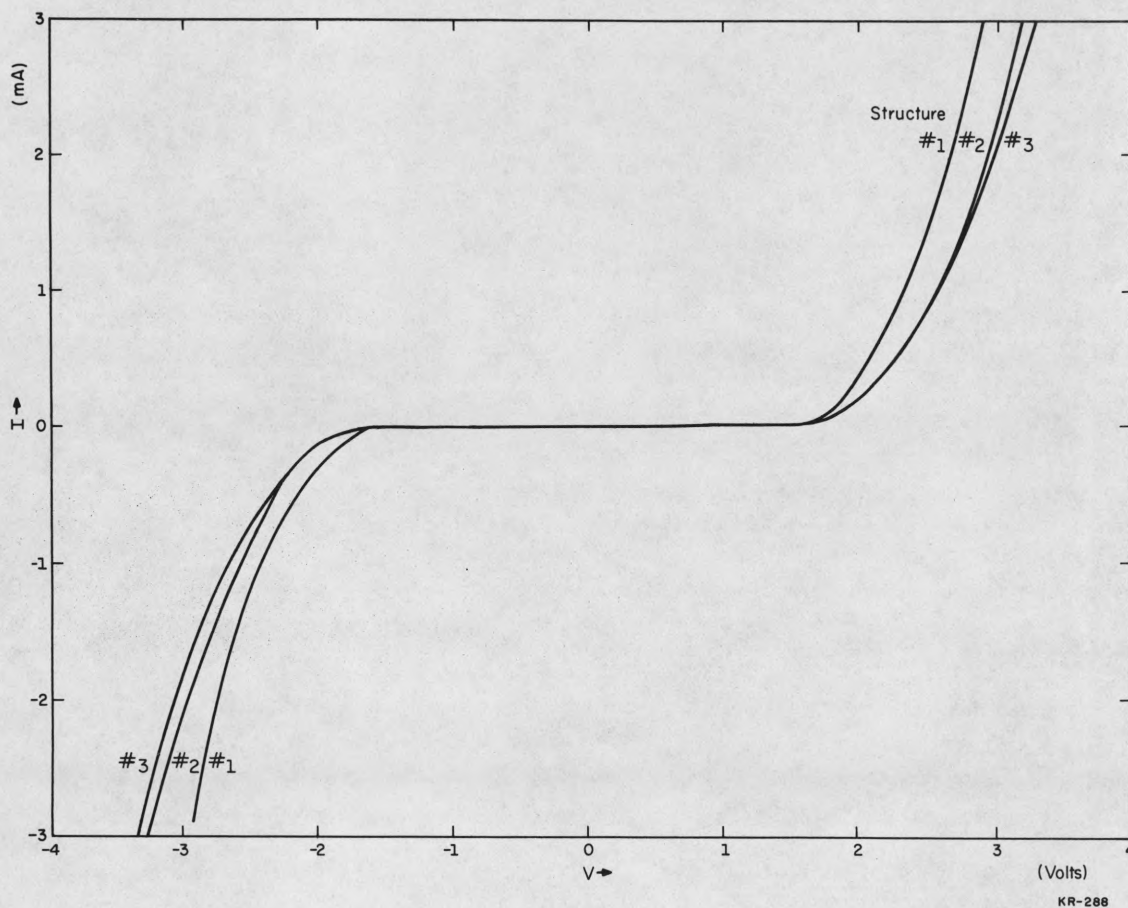

Figure 18. Slow sweep rate current-voltage relations for three Al-CeO-Al structures on the same slide. The cerium oxide (~100 Å) was electron beam deposited. M-I-M structures simultaneously deposited on the same slide showed dc resistance variations of at least this magnitude for all insulators tested.

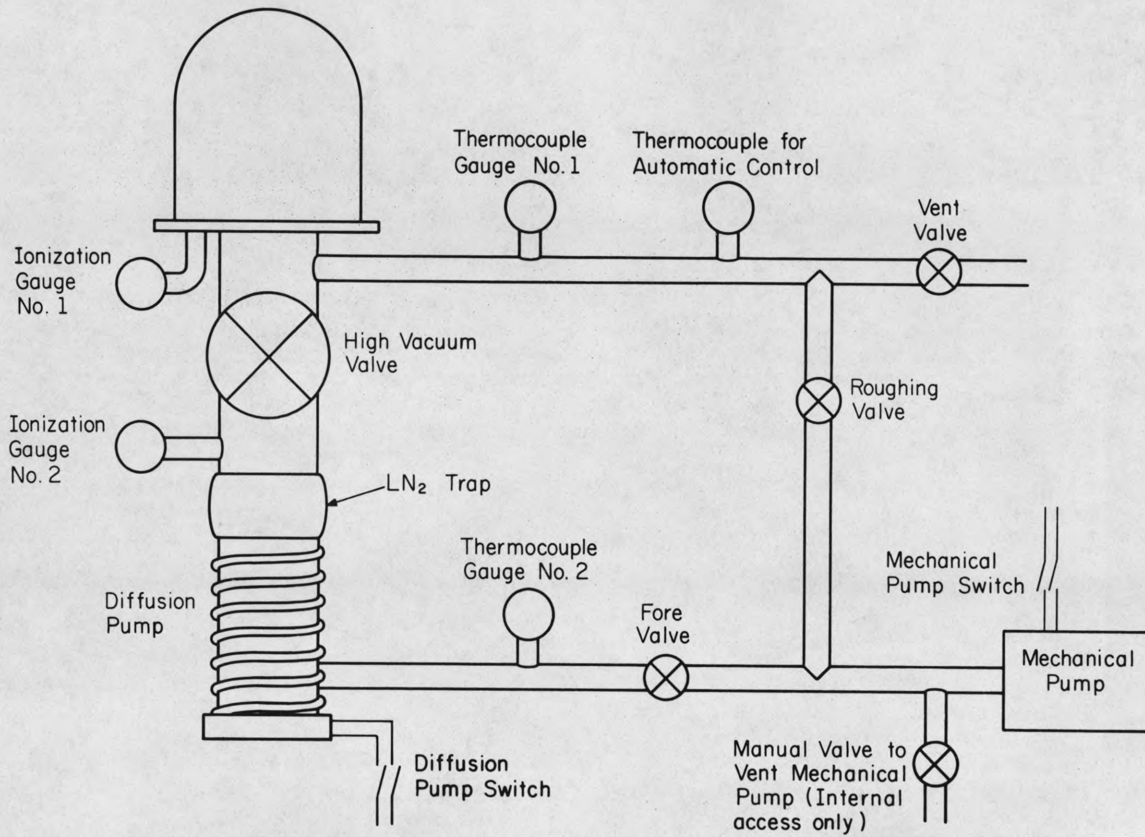

Figure 19. Schematic representation of the vacuum system to be shown in Fig. 20.

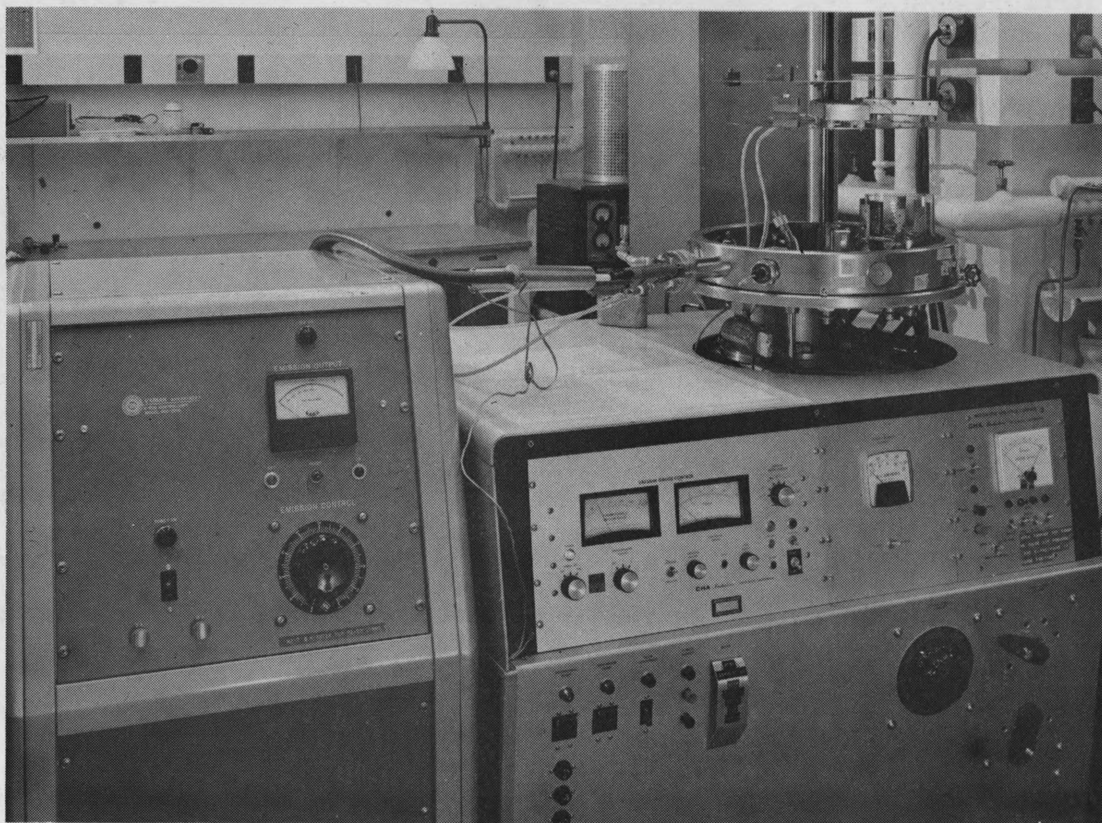

Figure 20. A commercial diffusion pumped vacuum system with bell jar raised, showing an electron beam deposition unit power supply.

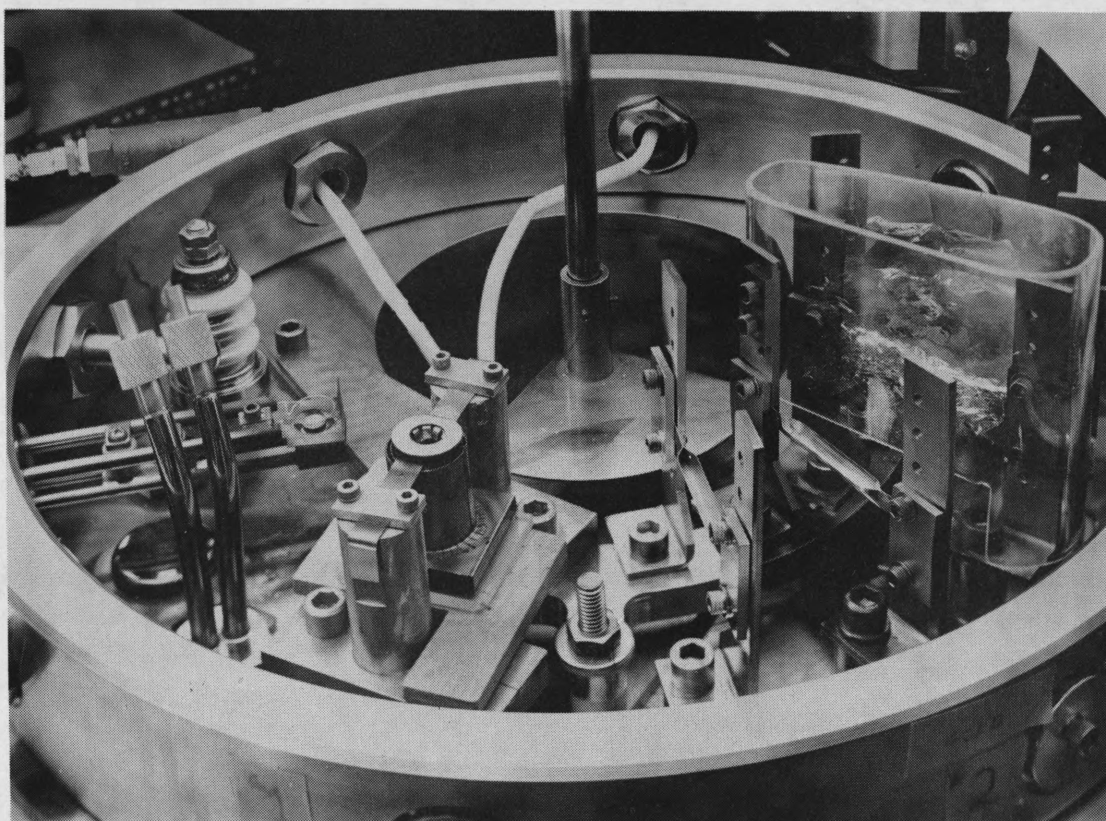

Figure 21 . Photograph of the hardware used for deposition. From left to right: high voltage feedthrough, micrometer leak valve, MRC electron beam gun, watercooling feedthrough, Drumheller source, and five tungsten or molybdenum boats.

APPENDIX

HIGH TEMPERATURE OXIDES AND NITRIDE

Dielectric Material	Density (CGS)	Resistivity (at 1000°K)	Soften or Melt Point (in °K)	Dielectric Constant (bulk)
Aluminum Oxide	3.37	$2x10^{8}$	2313	8
Beryllium Oxide	3.03	$1.5x10^{8}$	2843	
Borosilicate glass	2.52	$1x10^{2}$	828	
Cadmium Oxide	6.95		1773	
Calcium Oxide	3.35	$8x10^{6}$	2903	
Cerium Oxide	7.10	$1x10^{3}$	3073	
Ferroferric Oxide	3.14	$1x10^{0}$	1811	
Hafnium Oxide	9.68	$5x10^{7}$	3173	
Lanthanum Oxide	6.56		2483	
Lithium Oxide	2.01		1973	
Plutonium Oxide	11.46		2553	
Magnesium Oxide	3.77	$6x10^{9}$	3223	
Silicon Oxide	2.6	$8x10^{5}$	1708	4
Silicon Mon-oxide	2.1			6
Silicon Nitride	2.37		2228	4.2-6.2
Tellurium Dioxide	5.67		1005.8	
Thorium Diox-ide	10.0	$5x10^{5}$	3540	
Titanium Diox-ide	4.0	$4x10^{3}$	2113	100
Uranium Diox-ide	10.6	$1x10^{0}$	3153	
Vanadium Oxide	3.35	$1x10^{0}$	963	
Yttrium Oxide	5.05		2683	
Zinc Oxide		$1x10^{-1}$		
Zirconium Diox-ide	5.07	$1x10^{1}$	2983	

From Thermophysical Properties of High Temperature Solid Materials, ed. Y. S. Touloukion, Research Center, Purdue University.

REFERENCES

1. J. G. Simmons, "Electric Tunnel Effect between Dissimilar Electrodes Separated by a Thin Insulating Film," J. Appl. Phys. 34, 2581 (1963).

2. J. G. Simmons, "Generalized Formula for the Electric Tunnel Effect between Similar Electrodes Separated by a Thin Insulating Film," J. Appl. Phys. 34, 1793 (1963).

3. J. Lindmayer and C. Y. Wrigley, Fundamentals of Semiconductor Devices (Princeton, N.J.: Van Nostrand, 1964).

4. J. Lindmayer, "Current Transients in Insulators," J. Appl. Phys. 36, 196 (1965).

5. W. Shockley, "Electron Holes and Traps," Proc. IRE, 46, 973 (1958).

6. A. Rose, "Space-Charge-Limited Currents in Solids," Phys. Rev. 97, 1538 (1955).

7. A. Rose, Concepts in Photoconductivity and Allied Problems (New York: John Wiley, 1963).

8. C. Kittel, Introduction to Solid-State Physics (New York: John Wiley, 1959).

9. A. Rose, "Lifetime of Free Electrons and Holes in Solids," in Progress in Semiconductors (London: Heywood, 1957), vol. 2, p. 109.

10. J. Lindmayer, J. Reynolds, and C. Wrigley, "One-Carrier Space-Charge-Limited Current in Solids," J. Appl. Phys. 34, 809 (1963).

11. S. M. Hu, "Properties of Amorphous Silicon Nitride Films," J. Electrochemical Soc. 113, 693 (1966).

12. J. C. Fisher and I. Giaever, "Tunneling Through Thin Insulating Layers," J. Appl. Phys. 32, 172 (1961).

13. M. A. Lampert, "Injection Currents in Insulators," Proc. IRE, 50, 1781 (1962).

14. E. H. Snow, "Fowler-Nordheim Tunneling in SiO_2 Films," Solid State Communications, 5, 813 (1967).

15. R. Williams, "Photoemission of Electrons from Silicon into Silicon Dioxide," Phys. Rev. 140, A569 (1965).

16. T. E. Hartman, J. C. Blair, and R. Bauer, "Electrical Conduction Through SiO Films," J. Appl. Phys. 37, 2468 (1966).

17. P. R. Emtage and W. Tantraporn, Phys. Rev. Letters, 8, 267 (1962).

18. H. Schottky, Z. Physik, 15, 872 (1914).

19. W. Heitmann and E. Ritter, "Production and Properties of Vacuum Evaporated Films of Thorium Fluoride," Appl. Optics, 7, 307 (1968).

20. S. R. Pollack, "Schottky Yield Emission Through Insulating Layers," J. Appl. Phys. 34, 877 (1963).

21. P. P. Budenstein, "Breakdown Conduction in Thin Films of SiO, MgF_2, CaF_2, CeF_3, CeO_2 and Teflon," U.S. Dept. of Commerce Report N68-17300.

22. J. P. McKelvey, Solid State and Semiconductor Physics (New York: Harper & Row, 1966).

23. R. W. Roberts, "Clean Surfaces: Their Preparation and Characterization," Report No. 67-C-087, General Electric, Schenectady, N.Y.

24. W. F. Brunner and T. H. Batzer, Practical Vacuum Techniques (New York: Reinhold, 1965).

25. C. D. Stockbridge, "Resonance Frequency Versus Mass Added to Quartz Crystals," in Vacuum Microbalance Techniques (Murray Hill, N.J.: Bell Telephone Laboratories, 1966), vol. 5.

26. $(Gd_{.955},Eu_{.045})_2O_3$ supplied by Sylvania Chemical and Metallurgical Division, Towanda, Pa.

27. H. Y. Ku and F. G. Ullman, "Capacitance of Thin Dielectric Structures," J. Appl. Phys. 35, 265 (Feb. 1964).

28. MgO, CeO_2, MgF_2, CeF_3, TiO, and $ThOF_2$ supplied by Bendix Balzers, 5453 W. North Ave., Chicago, Ill.

29. N. Klein and H. Gafri, "The Maximum Dielectric Strength of Thin Silicon Oxide Films," IEEE Transactions on Electron Devices, 13 (1966).

30. SiO supplied by A. D. McKay, Inc., 198 Broadway, New York 38, N.Y.

31. Y. S. Touloukion, Thermophysical Properties of High Temperature Solid Materials (New York: Macmillan, 1967).

32. R. C. Weast, CRC Handbook of Chemistry and Physics, 47th ed. (Cleveland: Chemical Rubber Co., 1966-67).

Distribution List as of November 1, 1968

1 Dr A.A. Dougal
Asst Director (Research)
Ofc of Defense Res & Eng
Department of Defense
Washington, D.C. 20301

1 Office of Deputy Director
(Research and Technology)
ODD R&E-OSD
The Pentagon, Room 3-E-144
Washington, D.C. 20301

1 Director Advanced Research Projects Agency
Department of Defense
Washington, D.C. 20301

1 Director for Information Sciences
Advanced Research Projects Agency
Department of Defense
Washington, D.C. 20301

1 Director for Materials Sciences
Advanced Research Projects Agency
Department of Defense
Washington, D.C. 20301

1 Headquarters
Defense Communications Agency (333)
The Pentagon
Washington, D.C. 20305

20 Defense Documentation Center
Attn: TISIA
Cameron Station, Bldg 5
Alexandria, Virginia 22314

1 Director
National Security Agency
Attn: Librarian C-332
Fort George G. Meade, Maryland 20755

1 Weapons Systems Evaluation Group
Attn: Col Daniel W. McElwee
Department of Defense
Washington, D.C. 20305

1 National Security Agency
Attn: R4-James Tippett
Office of Research
Fort George G. Meade, Maryland 20755

1 Central Intelligence Agency
Attn: OCR/DD Publications
Washington, D.C. 20505

1 Colonel Kee
AFRSTE
Hqs, USAF
Room ID-429, The Pentagon
Washington, D.C. 20330

1 Aerospace Medical Division
AMD (AMRXI)
Brooks Air Force Base, Texas 78235

1 AUL3T-9663
Maxwell AFB, Alabama 36112

1 AFFTC (FTBPP-2)
Technical Library
Edwards AFB, Calif. 93523

1 Hq SAMSO (SMITA/Lt Nelson)
AF Unit Post Office
Los Angeles, California 90045

1 Lt Col Charles M. Waespy
Hq USAF (AFRDSD)
Pentagon
Washington, D.C. 20330

1 SSD (SSTRT/Lt Starbuck)
AFUPO
Los Angeles, California 90045

1 Det #6, OAR (LOOAR)
Air Force Post Office
Los Angeles, California 90045

1 ARL (ARIY)
Wright-Patterson AFB, Ohio 45433

1 Dr H.V. Noble
Air Force Avionics Laboratory
Wright-Patterson AFB, Ohio 45433

1 Mr Peter Murray
Air Force Avionics Laboratory
Wright-Patterson AFB, Ohio 45433

1 AFAL (AVTE/R.D. Larson)
Wright-Patterson AFB, Ohio 45433

2 Commanding General
Attn: STEWS-WS-VT
White Sands Missile Range
New Mexico, 88002

1 RADC (EMLAL01)
Griffiss AFB, New York 13442
Attn: Documents Library

1 Mr H.E. Webb (EMIA)
Rome Air Development Center
Griffiss AFB, New York 13442

1 Academy Library (DFSLB)
U.S. Air Force Academy
Colorado Springs, Colorado 80912

1 Mr Morton M. Pavane, Chief
AFSC Scientific and Liaison Office
26 Federal Plaza
New York, N.Y. 10007

1 Lt Col Bernard S. Morgan
Frank J. Seiler Research Laboratory
U.S. Air Force Academy
Colorado Springs Colorado 80912

1 Technical Library, AFETR
(ETV, MU-135)
Patrick AFB, Florida 32925

1 AFETR (ETLLG-1)
STINFO Office (For Library)
Patrick AFB, Florida 32925

1 Dr L. M. Hollingsworth
AFCRL (CRN)
L.G. Hanscom Field
Bedford, Massachusetts 01731

1 AFCRL (CRMZLR)
AFCRL Research Library, Stop 29
L.G. Hanscom Field
Bedford, Mass 01731

1 Colonel Robert E. Fontana
Dept of Electrical Engineering
Air Force Institute of Technology
Wright-Patterson AFB, Ohio 45433

1 Colonel A.D. Blue
RTD (RTTL)
Bolling Air Force Base, D.C. 20332

1 Dr I.R. Mirman
AFSC (SCT)
Andrews AFB, Maryland 20331

1 AFSC (SCTR)
Andrews AFB, Maryland 20331

1 Lt Col J.L. Reeves
AFSC (SCBB)
Andrews AFB, Maryland 20331

2 ESD (ESTI)
L.G. Hanscom Field
Bedford, Mass 01731

1 AEDC (ARO, INC)
Attn: Library/Documents
Arnold AFS, Tenn 37389

2 European Office of Aerospace Research
Shell Building
47 Rue Cantersteen
Brussels, Belgium

5 Lt Col Robert B. Lalisch
Chief, Electronics Division
Directorate of Engineering Sciences
Air Force Office of Scientific Research
Arlington, Virginia 22209

1 APGC (PGBS-12)
Elgin AFB, Florida 32542

1 U.S. Army Research Office
Attn: Physical Sciences Division
3045 Columbia Pike
Arlington, Virginia 22204

1 Research Plans Office
U.S. Army Research Office
3045 Columbia Pike
Arlington, Virginia 22204

1 Commanding General
U.S. Army Materiel Command
Attn: AMCRD-TP
Washington, D.C. 20315

1 Commanding General
U.S. Army Strategic Communication Command
Fort Huachuca, Arizona 85613

1 Commanding Officer
Army Materials & Mech. Res. Center
Watertown Arsenal
Watertown, Mass. 02172

1 Commanding Officer
U.S. Army Ballistics Research Laboratory
Attn: AMXRD-BAT
Aberdeen Proving Ground
Aberdeen, Maryland 21005

1 Commandant
U.S. Army Air Defense School
Attn: Missile Sciences Division
C & S Dept
P.O. Box 9390
Fort Bliss, Texas 79916

1 Commanding General
U.S. Army Missile Command
Attn: Technical Library
Redstone Arsenal, Alabama 35809

1 U.S. Army Munitions Command
Attn: Technical Information Command
Picatinney Arsenal
Dover, New Jersey 07801

1 Commanding Officer
Harry Diamond Laboratories
Attn: Dr Berthold Altman (AMXDO-TI)
Connecticut Ave & Van Ness St. N.W.
Washington, D.C. 20438

1 Commanding Officer
U.S. Army Security Agency
Arlington Hall
Arlington, Virginia 22212

1 Commanding Officer
U.S. Army Limited War Laboratory
Attn: Technical Director
Aberdeen Proving Ground
Aberdeen, Maryland 21005

1 Commanding Officer
Human Engineering Laboratories
Aberdeen Proving Grounds
Aberdeen, Maryland 21005

1 Commandant
U.S. Army Command & General Staff
College
Attn: Secretary
Fort Leavenworth, Kansas 66270

1 Commanding Officer
U.S. Army Research Office (Durham)
Attn: CRD-AA-IP (Richard O. Ulsh)
Box CM, Duke Station
Durham, North Carolina 27706

1 Librarian
U.S. Army Military Academy
West Point, New York 10996

1 The Walter Reed Institute of Research
Walter Reed Medical Center
Washington, D.C. 20012

1 Commanding Officer
U.S. Army Electronics R & D Activity
White Sands Missile Range
New Mexico 88002

1 Dr H. Robl
Deputy Chief Scientist
U.S. Army Research Office (Durham)
Box CM, Duke Station
Durham, North Carolina 27706

1 U.S. Army Mobility Equipment
Research & Development Center
Attn: Technical Document Center
Bldg 315
Fort Beloir, Virginia 22060

1 Mr Norman J. Field (AMSEL-RD-S)
Chief, Office of Science & Technology
U.S. Army Electronics Command
Fort Monmouth, New Jersey 07703

1 Mr Robert O. Parker
Executive Secretary,
JSTAC (AMSEL-XL-D)
Fort Monmouth, New Jersey 07703

1 Commanding General
U.S. Army Electronics Command
Fort Monmouth, New Jersey 07703
Attn: AMSEL-SC
RD-D
RD-G
RD-GF
RD-MAT
XL-D
XL-E (Dr K. Schwidta)
XL-C
XL-S
HL-D
HL-CTR
HL-CT-P (Dr W. McAfee)
HL-CT-L
HL-CT-O
HL-CT-I
HL-CT-A
NL-D
NL-A
NL-P-2 (D. Haratz)
NL-R
NL-S
KL-D
KL-E
KL-S
KL-T
VL-F (R.J. Niemela)
WL-D
1 Cy to each symbol listed.

1 Director Night Vision Laboratory
U.S. Army Electronics Command
Attn: HL-NV-II (Dr A.D. Schnitzler
Fort Belvoir, Virginia 22060

1 Components Research Laboratory
(P.E. Landis) Bldg 92
Harry Diamond Laboratories
Connecticut Ave & Van Ness St N.W.
Washington, D.C. 20438

1 Mr Edward Vaughan
Research & Engineering Directorate
U.S. Army Weapons Command
Rock Island, Illinois 61201

1 Commanding General
U.S. Army Missile Command
AMSMI-REX (W. Todd)
Redstone Arsenal, Ala 35809

3 Chief of Naval Research
Department of the Navy
Washington, D.C. 20360
Attn: Code 427

2 Naval Electronics Systems Command
ELEX 03
Falls Church, Virginia 22046

1 Naval Ship Systems Command
SHIP 031
Washington, D.C. 20360

1 Naval Ships Systems Command
SHIP 035
Washington, D.C. 20360

2 Naval Ordnance Systems Command
ORD 32
Washington, D.C. 20360

2 Naval Air Systems Command
AIR 03
Washington, D.C. 20360

2 Commanding Officer
Office of Naval Research Branch Office
Box 39, Navy No.100 F.P.O.
New York, New York 09510

1 Commanding Officer
Office of Naval Research Branch Office
219 South Dearborn Stree
Chicago, Illinois 60604

1 Commanding Officer
Office of Naval Reserve Branch Office
207 West 24th Street
New York, New York 10011

1 Commanding Officer
Office of Naval Research Branch Office
1030 East Green Street
Pasadena, California 91101

1 Commanding Officer
Office of Naval Research Branch Office
495 Summer Street
Boston, Massachusetts 02210

8 Director, Naval Research Laboratory
Technical Information Officer
Washington, D.C. 20360
Attn: Code 2000

1 Commander
Naval Air Development & Material Center
Johnsville, Pennsylvania 18974

2 Librarian
U.S. Naval Electronics Laboratory
San Diego, California 95152

1 Commanding Officer & Director
U.S. Naval Underwater Sound Laboratory
Fort Trumbull
New London, Connecticut 06840

1 Librarian
U.S. Naval Post Graduate School
Monterey, California 93940

1 Commander
U.S. Naval Air Missile Test Center
Point Magu, California 93041

1 Director
U.S. Naval Observatory
Washington, D.C. 20390

2 Chief of Naval Operations
OP-07
Washington, D.C. 20350

1 Director, U.S. Naval Security Group
Attn: G43
3801 Nebraska Avenue
Washington, D.C. 20390

2 Commanding Officer
Naval Ordnance Laboratory
White Oak, Maryland 21502

1 Commanding Officer
Naval Ordnance Laboratory
Corona, California 91720

1 Commanding Officer
Naval Ordnance Test Station
China Lake, California 93555

1 Commanding Officer
Naval Training Device Center
Orlando, Florida 32811

1 Commanding Officer
Naval Avionics Facility
Indianapolis, Indiana 46241

1 U.S. Naval Weapons Laboratory
Dahlgren, Virginia 22448

1 Weapons Systems Test Division
Naval Air Test Center
Patuxtent River, Maryland 20670
Attn: Library

1 Head, Technical Division
U.S. Naval Counter Intelligence
Support Center
Fairmont Building
4420 North Fairfax Drive
Arlington, Virginia 22203

1 Mr Charles Yost
Special Asst to the Director of Res.
National Aeronautics & Space Admin.
Washington, D.C. 20546

1 Dr H. Harrison, Code RRE
Chief, Electrophysics Branch
National Aeronautics & Space Admin.
Attn: Library C3/TDL
Green Belt, Maryland 20771

1 NASA Lewis Research Center
Attn: Library
21000 Brookpark Road
Cleveland, Ohio 22135

1 National Science Foundation
Attn: Program Director
Engineering System Program ENG
1800 G. Street, N.W.
Washington, D.C. 20550

1 U.S. Atomic Energy Commission
Division of Technical Information Ext.
P.O. Box 62
Oak Ridge, Tenn. 37831

1 Los Alamos Scientific Laboratory
Attn: Reports Library
P.O. Box 1663
Los Alamos, New Mexico 87544

2 NASA Scientific & Technical Inform. Fac.
Attn: Acquisitions Branch (S/AK/DL)
P.O. Box 33
College Park, Maryland 20740

1 Director
Research Laboratory of Electronics
Massachusetts Institute of Technology
Cambridge, Mass 02139

1 Polytechnic Institute of Brooklyn
55 Johnson Street
Brooklyn, New York 11201
Attn: Mr Jerome Fox
Research Coordinator

1 Director
Columbia Radiation Laboratory
Columbia University
538 West 120th Street
New York, New York 10027

1 Director
Coordinated Science Laboratory
University of Illinois
Urbana, Illinois 61801

1 Director
Stanford Electronics Laboratories
Stanford University
Stanford, California 94305

1 Director
Electronics Research Laboratory
University of California
Berkeley, California 94720

1 Director
Electronic Sciences Laboratory
University of Southern California
Los Angeles, California 90007

1 Electronics Research Center
University of Texas at Austin
Engr-Science Bldg 110
Austin, Texas 78712

1 Division of Engineering &
Applied Physics
210 Pierce Hall
Harvard University
Cambridge, Massachusetts 02138

1 Aerospace Corporation
P.O. Box 95085
Los Angeles, California 90045
Attn: Library Acquisition Group

1 Professor Nicholas George
California Inst. of Technology
Pasadena, California 91109

1 Aeronaurics Library
Graduate Aeronautical Laboratories
California Institute of Technology
1201 E. California Blvd
Pasadena, California 91109

1 Director, USAF Project Rand
Via: Air Force Liaison Office
The Rand Corporation
1700 Main Street
Santa Monica, California 90406

1 Hunt Library
Carnegie Institute of Technology
Schenley Park, Pittsburgh, Pa. 15213

1 Syracuse University
Dept of Electrical Engineering
Syracuse, New York 13210

1 Yale University
Engineering Dept
New Haven, Connecticut 06520

1 Airborne Instruments Laboratory
Deerpark, New York 11729

1 Bendix Pacific Division
11600 Sherman Way
North Hollywood, California 91605

1 General Electric Co
Research Laboratories
Schenectady, New York 12301

1 Lockheed Aircraft Corp
P.O. Box 504
Sunnyvale, California 94088

1 Raytheon Co
Bedford, Mass 01730
Attn: Librarian

1 Dr G. J. Murphy
The Technological Institute
Northwestern University
Evanston, Illinois 60201

1 Dr John C, Hancock, Director
Electronics Systems Research Laboratory
Purdue University
Lafayette, Indiana 47907

1 Director
Microwave Laboratory
Stanford University
Stanford, California 94305

1 Emil Schafer, Head
Electronics Properties Infor. Center
Hughes Aircraft Co
Culver, California 90230

1 The John Hopkins University
Applied Physics Laboratory
8621 Georgia Avenue
Silver Springs, Maryland 20910
Attn: Boris W. Kuvshinoff
Document Librarian

1 Dr Leo Young
Stanford Research Institute
Menlo Park, California 94025

1 Mr Henry Bachmann
Assistant Chief Engineer
Wheeler Laboratories
122 Cutterhill Road
Great Neck, New York 11021

1 School of Engineering Sciences
Arizona State University
Tempe, Arizona 85281

1 Engineering & Math Sciences Library
University of California at Los Angeles
405 Hilgred Avenue
Los Angeles, California 90024

1 California Institute of Technology
Pasadena, California 91109
Attn: Documents Library

1 University of California
Santa Barbara, California 93106
Attn: Library

1 Carnegie Institute of Technology
Electrical Engineering Dept
Pittsburgh, Pa 15213

1 University of Mighigan
Electrical Engineering Dept
Ann Arbor, Michigan 48104

1 New York University
College of Engineering
New York, N.Y. 10019

1 Dept of Electrical Engineering
Texas Technological College
Lubbock, Texas 79409

1 IBM Technical Info. Retrieval Center
International Business Machines Corp.
Armonk, New York 10504

1 Commander
Test Command (TCDT-E)
Defense Atomic Support Agency
Sandia Base
Albuquerque, New Mexico 87115

1 Commanding General
U.S. Army Weapons Command
Rock Island, Ill 61201
Attn: ANSWE-RDR (Gerald Reinsmith)

1 Col E.P. Gaines, ACDA/FO
1901 Pennsylvania Ave, N.W.
Washington, D.C. 20451

1 Mr Billy Locke
Plans Directorate
USAF Security Service
Kelly Air Force Base, Texas 78241

1 W.A. Eberspacher
Technical Consultant
Systems Integration
Code 5340A, Box 15
Naval Missile Center
Point Magu, California 93041

1 Director of Faculty Research
Department of the Air Force
USAF Academy
Colorado 80840

1 Lt Col Richard Bennett
AFRDD
The Pentagon
Washington, D.C. 20301

1 Weapons Systems Evaluation Group
Attn: Col John B. McKinney
410 Army-Navy Drive
Arlington, Virginia 22202

1 Mr M. Zane Thornton
National Library of Medicine
8600 Rockville Pike
Bethesda, Maryland 22014

Security Classification

DOCUMENT CONTROL DATA - R & D

(Security classification of title, body of abstract and indexing annotation must be entered when the overall report is classified)

1. ORIGINATING ACTIVITY *(Corporate author)*	2a. REPORT SECURITY CLASSIFICATION
University of Illinois Coordinated Science Laboratory Urbana, Illinois 61801	Unclassified 2b. GROUP

3. REPORT TITLE

ELECTRICAL PROPERTIES OF SOME VACUUM DEPOSITED INSULATING FILMS

4. DESCRIPTIVE NOTES *(Type of report and inclusive dates)*

5. AUTHOR(S) *(First name, middle initial, last name)*

REILLY, Owen J.

6. REPORT DATE	7a. TOTAL NO. OF PAGES	7b. NO. OF REFS
January, 1969	55	32

8a. CONTRACT OR GRANT NO.	9a. ORIGINATOR'S REPORT NUMBER(S)
DAAB-07-67-C-0199; also in part Army b. PROJECT NO. DAAK-02-67-C-0546.	R-403
c.	9b. OTHER REPORT NO(S) *(Any other numbers that may be assigned this report)*
d.	

10. DISTRIBUTION STATEMENT

Distribution of this report is unlimited.

11. SUPPLEMENTARY NOTES	12. SPONSORING MILITARY ACTIVITY
	Joint Services Electronics Program thru U.S. Army Electronics Command Ft. Monmouth, New Jersey 07703

13. ABSTRACT

Materials can be classified as conductors, semiconductors, or insulators. The distinguishing difference among these classes is the resistivity. Conductors generally have resistivities of the order of 10^{-5} ohm-cm; semiconductors fall in a range around 1 ohm-cm; and insulators have resistivities near 10^{10} ohm-cm. This large difference in resistivity of the three classes of materials is the basis of their engineering applications. The resistivities of all three classes may be functions of many parameters, including temperature, purity, conditions of preparation, and the field strengths applied to them. The experimentally determined resistivities for a group of vacuum deposited thin film insulators will be presented in this paper.

DD FORM 1 NOV 65 1473

Security Classification

Security Classification

14. KEY WORDS	LINK A		LINK B		LINK C	
	ROLE	WT	ROLE	WT	ROLE	WT
Thin Film						
Insulators						
Vacuum Deposition						
Resistivities						

Security Classification